The Natural Metabolite 4-Cresol Improves Glucose Homeostasis and Enhances β-Cell Function

Francois Brial, Fawaz Alzaid, Kazuhiro Sonomura, Yoichiro Kamatani, Kelly Meneyrol, Aurelie Le Lay, Noémie Péan, Lyamine Hedjazi, Taka-Aki Sato, Nicolas Venteclef, et al.

HAL Id: hal-03089353

https://cnrs.hal.science/hal-03089353

Submitted on 28 Dec 2020

Article

The Natural Metabolite 4-Cresol Improves Glucose Homeostasis and Enhances β-Cell Function

Graphical Abstract
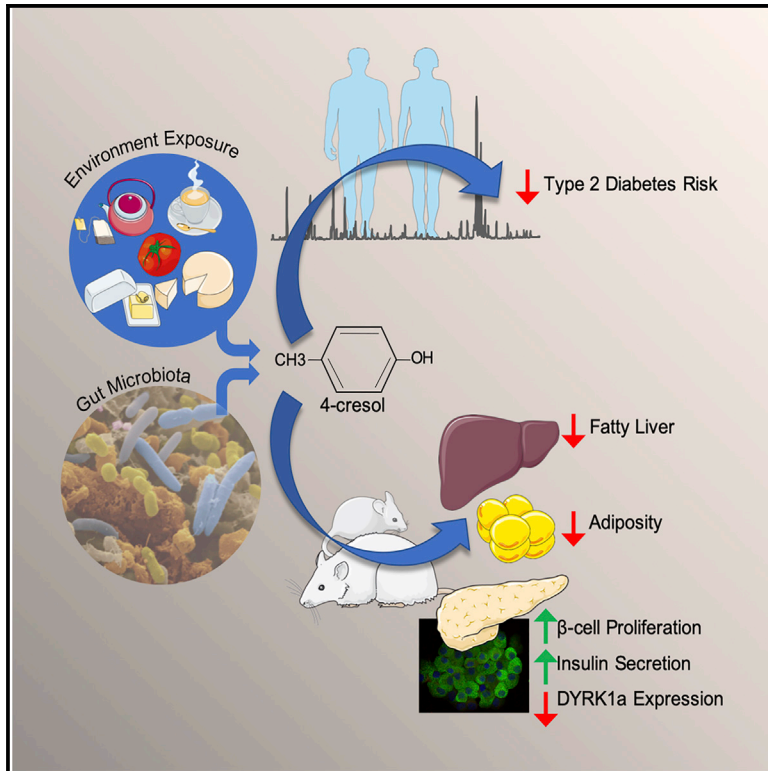
Authors

Francois Brial, Fawaz Alzaid, Kazuhiro Sonomura, ..., Fumihiko Matsuda, Pierre Zalloua, Dominique Gauguier

Correspondence

pierre.zalloua@lau.edu.lb (P.Z.),
dominique.gauguier@crc.jussieu.fr (D.G.)

In Brief

Brial et al. identify the inverse correlation between diabetes and serum 4-cresol, a metabolite present in the environment and produced by intestinal bacteria. The administration of 4-cresol in models of diabetes reduces obesity and liver fat, improves glycemic control, and stimulates insulin secretion and β-cell proliferation.

Highlights

- Serum concentrations of 4-cresol are inversely correlated with type 2 diabetes

- Non-toxic dose of 4-cresol reduces adiposity, glucose intolerance, and liver fat

- 4-Cresol stimulates insulin secretion and β-cell proliferation *in vivo* and *in vitro*

- 4-Cresol downregulates pancreatic and islet expression of the kinase DYRK1A

CellPress

The Natural Metabolite 4-Cresol Improves Glucose Homeostasis and Enhances β-Cell Function

Francois Brial,[1] Fawaz Alzaid,[2] Kazuhiro Sonomura,[3,4] Yoichiro Kamatani,[3] Kelly Meneyrol,[5] Aurélie Le Lay,[1] Noémie Péan,[1] Lyamine Hedjazi,[1] Taka-Aki Sato,[4] Nicolas Venteclef,[2] Christophe Magnan,[5] Mark Lathrop,[6] Marc-Emmanuel Dumas,[7] Fumihiko Matsuda,[3] Pierre Zalloua,[8,*] and Dominique Gauguier[1,3,6,9,*]

[1]Université de Paris, INSERM UMR 1124, 75006 Paris, France
[2]Sorbonne Université, Université Paris Descartes, INSERM UMR_S 1138, Cordeliers Research Centre, 75006 Paris, France
[3]Center for Genomic Medicine, Kyoto University Graduate School of Medicine, Kyoto 606-8501, Japan
[4]Life Science Research Center, Technology Research Laboratory, Shimadzu, Kyoto 604-8511, Japan
[5]Université de Paris, Unit of Functional and Adaptive Biology, UMR 8251, CNRS, 4 rue Marie Andrée Lagroua Weill-Halle, 75013 Paris, France
[6]McGill University and Genome Quebec Innovation Centre, 740 Doctor Penfield Avenue, Montreal, QC H3A 0G1, Canada
[7]Imperial College London, Section of Biomolecular Medicine, Division of Computational and Systems Medicine, Department of Surgery and Cancer, Faculty of Medicine, Sir Alexander Fleming Building, London SW7 2AZ, UK
[8]Lebanese American University, School of Medicine, Beirut 1102 2801, Lebanon
[9]Lead Contact
*Correspondence: pierre.zalloua@lau.edu.lb (P.Z.), dominique.gauguier@crc.jussieu.fr (D.G.)
https://doi.org/10.1016/j.celrep.2020.01.066

SUMMARY

Exposure to natural metabolites contributes to the risk of cardiometabolic diseases (CMDs). Through metabolome profiling, we identify the inverse correlation between serum concentrations of 4-cresol and type 2 diabetes. The chronic administration of nontoxic doses of 4-cresol in complementary preclinical models of CMD reduces adiposity, glucose intolerance, and liver triglycerides, enhances insulin secretion *in vivo*, stimulates islet density and size, and pancreatic β-cell proliferation, and increases vascularization, suggesting activated islet enlargement. *In vivo* insulin sensitivity is not affected by 4-cresol. The incubation of mouse isolated islets with 4-cresol results in enhanced insulin secretion, insulin content, and β-cell proliferation of a magnitude similar to that induced by GLP-1. In both CMD models and isolated islets, 4-cresol is associated with the downregulated expression of the kinase DYRK1A, which may mediate its biological effects. Our findings identify 4-cresol as an effective regulator of β-cell function, which opens up perspectives for therapeutic applications in syndromes of insulin deficiency.

INTRODUCTION

Type 2 diabetes (T2D) is a multifactorial disorder resulting from the effects of many genes interacting with environmental factors (Barroso and McCarthy, 2019; Franks and McCarthy, 2016). Genome-wide association studies have revealed many T2D risk loci, which explain a modest proportion of the disease risk. Growing evidence supports a role of exposure to xenobiotics, including products of gut microbial meta-

bolism and environmental pollutants, in the etiology of chronic diseases (Barouki et al., 2018). For example, food additives, contact materials, and neoformed contaminants increase the risk of cardiovascular diseases (Srour et al., 2019). Metabolomics is a technology designed to quantitatively and qualitatively analyze a broad range of small molecules, which are molecular endpoints of genome expression and its adaptation to environmental exposures (Nicholson et al., 2002). Metabolic endophenotypes generated by metabolomic-based phenotyping and metabotyping (Gavaghan et al., 2000) can be used as biomarkers underlying disease etiology (Brindle et al., 2002; Kirschenlohr et al., 2006) and help us to understand disease pathogenesis and develop relevant therapeutic solutions.

To identify the metabolites associated with the risk of T2D, we applied a targeted gas chromatography coupled to mass spectrometry (GC-MS) approach to the profiling of 101 serum metabolites in a human study population. We identified a metabotype of 6 metabolites associated with T2D, including the metabolite 4-cresol, previously unreported in metabolomic studies of T2D, which was negatively correlated with T2D and may underlie mechanisms of disease resistance. Chronic administration of 4-cresol in preclinical models of spontaneous or experimentally induced insulin resistance resulted in significantly improved glucose homeostasis, enhanced glucose-stimulated insulin secretion *in vivo*, reduced adiposity, and increased pancreas weight. Further physiological, histological, and molecular analyses in 4-cresol-treated animals indicated enhancement of both β-cell proliferation and pancreas vascularization, which may be mediated by the downregulated expression of the kinase DYRK1A (Becker et al., 1998) and the upregulated expression of SIRT1. Our findings illustrate the contribution of metabolomics in defining risk markers for chronic diseases through the identification of 4-cresol as a regulator of T2D endophenotypes with potential therapeutic applications.
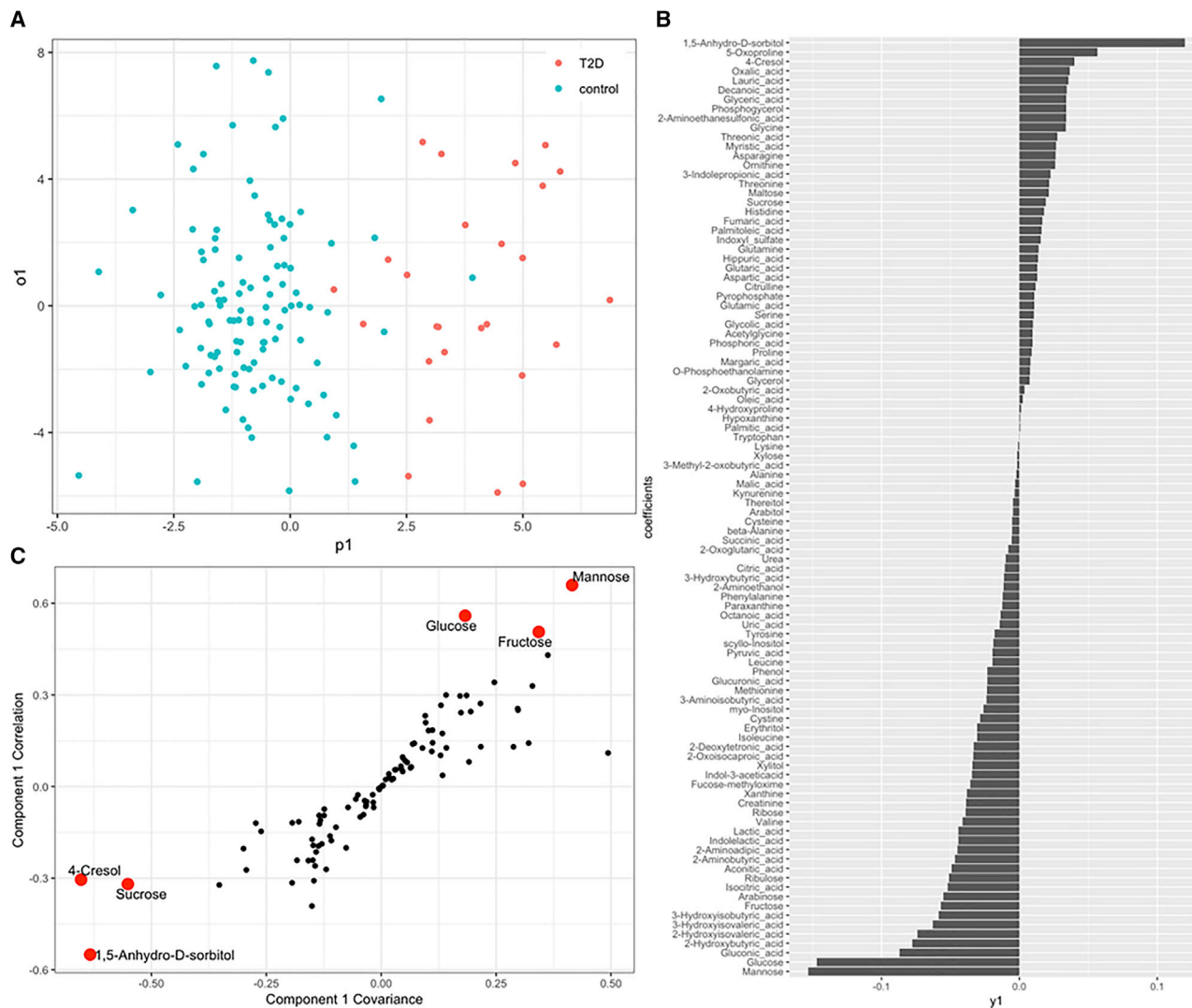
Figure 1. Association Analysis of Metabolites with Type 2 Diabetes

Metabolomic profiling was used to identify the association between the abundance of serum metabolites and type 2 diabetes (T2D) in the study population (n = 137).

(A) Orthogonal partial least-squares discriminant analysis (O-PLS-DA) scores plot illustrates separation between diabetic and control individuals.

(B) 4-Cresol was among the metabolites showing the highest negative association with T2D.

(C) The S-plot indicates the 6 metabolites (highlighted in red) showing the highest absolute contribution to the association, with absolute values of covariance or correlation > 0.5.

Statistics were corrected for multiple comparisons and adjusted for age and gender.

RESULTS

Metabolic Profiling Identifies Negative Correlation between 4-Cresol and T2D

Targeted metabolomic profiling was applied to test associations between variations in circulating metabolites and T2D risk in the study population. The method allowed semiquantitative analysis of 101 metabolites from GC-MS spectra of serum samples from cases and controls, including 36 amino acids, 32 organic acids, 20 sugars, and other molecular compounds (e.g., nucleobases) (Table S1).

Orthogonal partial least-squares discriminant analysis (O-PLS-DA) was initially applied to GC-MS data to stratify the population based on T2D with goodness-of-fit value R^2Y of 0.687, and goodness-of-prediction value Q^2Y of 0.519 (Figure 1A). Both goodness values showed strong statistical significance (p < 0.0001) after 10,000 times permutation. 4-Cresol showed the 4th highest negative loading value for T2D (Figure 1B). The S-plot, which summarizes model coefficients supporting this discrimination (Wiklund et al., 2008), highlighted 3 metabolites significantly positively correlated with T2D (glucose, mannose, fructose) and 3 metabolites negatively correlated with the disease (1,5-anhydro-D-sorbitol, 4-cresol, sucrose) (Figure 1C). We also identified a marginally significant correlation between 4-cresol and reduced body mass index (p = 2.2 × 10^{-2}).

These results demonstrate the power of systematic and simultaneous metabolomic-based profiling of a large series of metabolites to identify metabotypic endophenotypes associated with diseases and point to 4-cresol as a potentially important metabolite associated with reduced T2D risk.

4-Cresol Treatment Improves Glucose Homeostasis and Reduces Body Weight Gain in Mice

We prioritized *in vivo* experimental validation of the clinical association on 4-cresol, whose biological role in metabolism and potential benefits for T2D are unknown. We chronically treated mice fed a control diet or a high-fat diet (HFD) with subcutaneous infusion of a solution of 4-cresol 0.04 M, corresponding to ~0.5 mg/kg/day, for 42 days using an experimental design illustrated in Figure S1. Subcutaneous treatment was preferred over dietary supplementation or oral gavage to avoid the possible conversion of 4-cresol by gut bacteria or enterocytes, to control permanent delivery of 4-cresol over a long period, and to reduce the stress induced by animal handling that gavage requires. This delivery method also avoided the possible toxic effects of this volatile compound that are observed at much higher doses (240–2,000 mg/kg/day) on neurological function, liver function, and respiratory epithelium (Andersen, 2006). As expected, mice fed an HFD rapidly gained more weight than did mice fed a control diet and developed fasting hyperglycemia and marked glucose intolerance (Figures 2A–2F). Glycemia after the glucose challenge, cumulative glycemia during the intraperitoneal glucose tolerance test (IPGTT), and the ΔG parameter were significantly more elevated in mice fed an HFD than in controls (Figures 2C–2F). Fasting insulin and glucose-induced insulin secretion were not significantly affected by HFD (Figure 2G).

The chronic infusion of mice fed a control diet with 4-cresol resulted in a progressive reduction in body weight when compared to mice treated with saline (Figure 2A). This effect became significant after 4 weeks of 4-cresol treatment and remained significant until the end of the experiment. The index body mass was also significantly decreased after 6 weeks of 4-cresol treatment (Figure 2B). Glucose tolerance was improved by 4-cresol, as indicated by the significant reduction in both acute glycemic response to the glucose challenge and cumulative glycemia during the IPGTT when compared to saline-treated mice (Figures 2C and 2D). 4-Cresol infusion resulted in a significant increase in the glucose-stimulated secretion of insulin (Figure 2G) and C-peptide (Figure 2H) when compared to controls.

The effect of 4-cresol on reduced body weight, improved glycemic control, and stimulated secretion of insulin and C-peptide in response to glucose was also strongly significant in HFD-fed mice (Figures 2A–2H). In addition, 4-cresol treatment in fat-fed mice induced a strong reduction in fasting glycemia (Figure 2F), in the ΔG parameter, which was normalized to the level of mice fed a chow diet (CHD) and treated with saline (Figure 2E), and in fasting hyperinsulinemia (Figure 2G) when compared to HFD-fed mice infused with saline.

In Vivo 4-Cresol Treatment Alters Organ Weight and Reduces Liver Triglycerides

To further characterize the effects of 4-cresol on phenotypes relevant to T2D and obesity, we measured organ and tissue weights and analyzed phenotypes frequently associated with obesity (e.g., fatty liver disease) in the mouse groups. After 7 weeks of HFD, mice exhibited significantly elevated adiposity, which was calculated as the ratio of the retroperitoneal fat pad weight to body weight (Figure 2I) and reduced heart weight (Figure S2) when compared to mice fed CHD. Liver triglycerides levels were markedly increased by HFD (Figure 2L).

In both diet groups, the chronic administration of 4-cresol over 6 weeks resulted in a significant reduction in the adiposity index (Figure 2I) and increased pancreas weight by 48.9% (Figure 2J) when compared to mice treated with saline. Heart and kidney weights were not affected by 4-cresol (Figure S2). Liver weight was reduced in HFD-fed mice treated with 4-cresol (Figure 2K). 4-Cresol treatment resulted in a systematic and dramatic reduction in liver triglycerides content in both diet groups (Figure 2L).

These data demonstrate the beneficial effects of the chronic administration of 4-cresol *in vivo* in mice on glucose homeostasis, thus validating our results from metabolomic profiling in patients, and extend the characterization of its effects on reduced obesity and liver triglycerides.
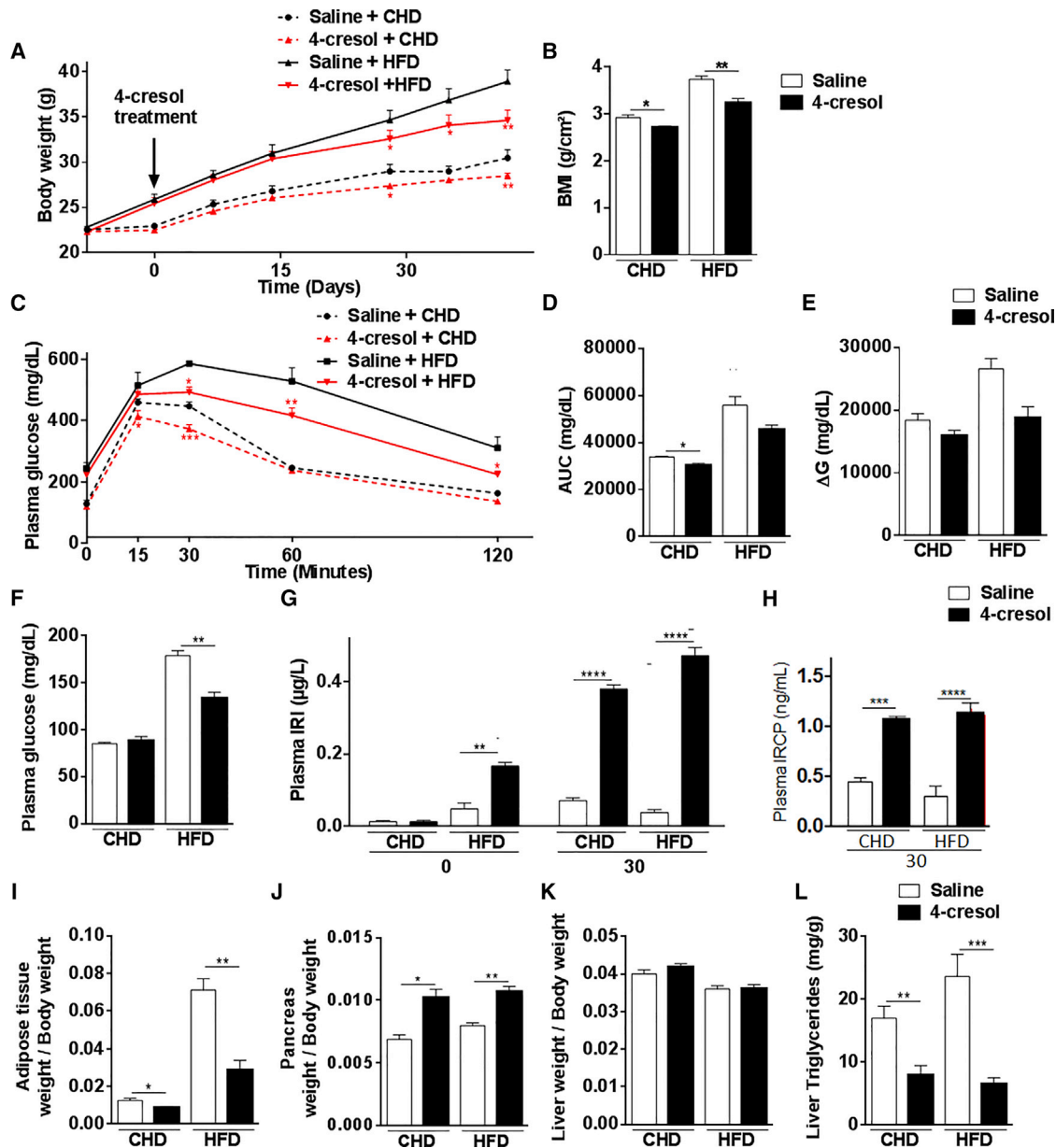
Treatment with 4-Cresol or Its Derivative 4-Methylcatechol Has Similar Biological Effects

We then investigated whether these physiological effects are specific to 4-cresol or can be replicated with the products of 4-cresol conversion, thus structurally related to 4-cresol (Figure S3). We repeated the *in vivo* phenotypic screening in control and HFD-fed mice treated with 4-methylcatechol (4-MC), a product of 4-cresol through enzymatic reactions potentially involving bacterial mono-oxygenase, dioxygenase, and cyclo-isomerase (Kolomytseva et al., 2007). The chronic treatment of mice fed a CHD or an HFD with 4-MC induced a strong reduction in body growth and in body mass index (Figures S3A and S3B), significant improvement in glycemic control on both diets, as demonstrated by improved glucose tolerance, reduced fasting glycemia and cumulative glycemia and ΔG during the IPGTT (Figures S3C–S3F), and increased the secretion of insulin (Figure S3G) and C-peptide (Figure S3H) when compared to mice treated with saline. The treatment of mice fed a control diet or an HFD with 4-MC induced a significant reduction in adiposity, liver weight, and liver triglycerides and increased pancreas weight (Figures S2I–S2L). These results indicate that 4-cresol and 4-MC have very similar effects in several tissues and may regulate the same biological mechanisms in these tissues.

4-Cresol and 4-Methylcatechol Reduce Food Intake in Fat-Fed Mice

To verify these results and provide an explanation for the reduction in adiposity induced by 4-cresol and 4-methylcatechol, we carried out an independent replication study in C57BL/6J mice treated with these metabolites using the same experimental design (Figure S1) in addition to records of food intake. We fully replicated the significant effects of chronic treatment with 4-cresol and 4-methylcatechol on reduced adiposity, improved glucose tolerance, and, most

Figure 2. Chronic Administration of 4-Cresol Improves Glucose Homeostasis and Reduces Obesity in C57BL6/J Mice

(A–L) The effects of 6-week-long administration of 4-cresol *in vivo* in mice fed a control chow (CHD) or high-fat diet (HFD) were tested on body weight (A), body mass index (BMI) (B), glucose tolerance profile (C) and indices (D,E), fasting glycemia (F), glucose-stimulated secretion of insulin (G) and C-peptide (H), ratios of the weight of adipose tissue (I), pancreas (J) and liver (K) to body weight, and liver triglycerides content (L).

BMI was calculated as body weight divided by squared anal-to-nasal length. Area under the curve (AUC) was calculated as the sum of plasma glucose values during the IPGTT. ΔG is the AUC over the baseline value integrated over the 120 min of the test. All of the measures are from 6 mice per group. Data were analyzed using the unpaired Mann-Whitney test. Results are means ± SEMs. *p < 0.05; **p < 0.01; ***p < 0.001; ****p < 0.0001; significantly different from relevant controls. IRCP, immunoreactive C-peptide; IRI, immunoreactive insulin.

important, enhanced glucose-induced insulin secretion and pancreas weight in both CHD- and HFD-fed mice (Figures S4 and S5). In CHD-fed mice, energy intake was similar in mice treated with the metabolites and in saline-treated mice (Figure S6A). In contrast, in HFD-fed mice, energy intake was significantly reduced at the second day of recording in both

mouse groups treated with the metabolites when compared to saline-treated mice (Figure S6B). Changes in plasma concentrations of the satiety hormone leptin and the appetite hormone ghrelin at this time point cannot account for the reduction in food intake in HFD-fed mice treated with the metabolites, even though plasma leptin tends to be more

elevated in mice treated with 4-methylcatechol than in controls (p = 0.10) (Figure S6B).

Insulin Sensitivity Is Not Affected by Chronic Administration of 4-Cresol or Its Derivative 4-Methylcatechol

To test a possible effect of 4-cresol and 4-MC on *in vivo* insulin sensitivity, insulin tolerance tests were carried out in mice treated with these metabolites or saline for 4 weeks. Insulin injection induced similar decreases in glycemia in mice treated with the metabolites and in mice infused with saline and fed a CHD (Figure S7A) or an HFD (Figure S7B). Glycemia remained lower in CHD-fed mice infused with the metabolites than in control mice, suggesting increased insulin sensitivity *in vivo* in response to chronic stimulation with 4-cresol and 4-MC (Figure S7A).

Chronic Administration of 4-Cresol Ameliorates Adipose Tissue and Liver Histological Features

To characterize the effects of 4-cresol on adiposity and lipid metabolism at the organ level, we carried out histological analyses of adipose tissue and liver in the 4 mouse groups (Figure S8). HFD feeding induced a strongly significant increase (84.8%) in adipocyte size (56.27 ± 0.47 in CHD-fed mice and 104.00 ± 1.41 in HFD-fed mice) (Figures S8A and S8B), which is consistent with increased adiposity in response to fat feeding. In CHD-fed mice, 4-cresol induced a slight reduction in adipocyte diameter when compared to saline-treated mice (53.97 ± 0.39, p = 0.006). Remarkably, 4-cresol administration in HFD-fed mice led to a strongly significant reduction in adipocyte size (66.22 ± 0.70, p < 0.0001) to a level close to that of saline-treated CHD-fed controls (Figures S8A and S8B).

The occurrence of liver structural lesions resembling non-alcoholic fatty liver disease (NAFLD) is a phenotypic hallmark consistently observed in obese mice fed HFDs in our experimental conditions (Dumas et al., 2006). To investigate the effect of 4-cresol on these defects and test the histological relevance of reduced liver triglycerides observed in mice treated by 4-cresol (Figure 2K), we carried out liver histology in the 4 mouse groups. HFD feeding induced a strongly significant 4.27-fold increase in liver fat content determined by oil red O staining of liver sections (Figures S8C and S8D). In response to 4-cresol infusion, liver fat content was strongly reduced by 40.7% in HFD-fed mice (p = 0.009) to levels similar to CHD-fed controls treated with saline (Figure S8D).

Gene Expression Changes Induced by Chronic 4-Cresol Treatment in Adipose Tissue

To investigate the molecular changes potentially underlying morphological changes in adipose tissue in response to 4-cresol treatment, we analyzed the expression of a selection of genes known to regulate adipocyte function in obesity (Figure S9). Expressions of sirtuin 1 (Sirt1), caveolin 2 (Cav2), hormone-sensitive lipase (Hsl), and patatin-like phospholipase domain containing 2 (Pnpla2, Atgl) were significantly stimulated by 4-cresol in CHD-fed mice, whereas uncoupling protein 1 (Ucp1) expression was markedly downregulated. The expression of Hsl and Pnpla2 remained significantly upregulated by 4-cresol in HFD-fed mice when compared to saline-treated fat-

fed mice, and Ucp1 was significantly downregulated in these mice when compared to both HFD-fed mice treated with saline and CHD-fed mice treated with 4-cresol.

Chronic Administration of 4-Cresol Increases Pancreatic Vascularization and Islet Density and Promotes β-Cell Proliferation

One of our most striking observations was the massive effect of 4-cresol on increased pancreas weight in both diet groups (Figure 2J), which we analyzed further through histology of pancreas sections. To test whether islet structure was affected by 4-cresol, we focused histopathology analyses on islets in sections stained by hematoxylin&eosin. Fat feeding did not affect the overall insulin-positive area (58.95 ± 11.75 in CHD-fed mice; 109.03 ± 24.15 in HFD-fed mice, p = 0.071) (Figures 3A and 3B), but increased β-cell mass and islet density (Figures 3C–3E). 4-Cresol administration was associated with a strong increase in the insulin-positive area, β-cell mass, and islet density in mice fed a CHD (185.40 ± 22.95) or an HFD (171.90 ± 21.62), but the effect was statistically significant only in CHD-fed mice. We noted that islets in the pancreas sections of cresol-treated mice were predominantly located in the close vicinity of the vasculature (Figure 3D).

To test whether 4-cresol would also affect pancreatic α-cells producing glucagon, we quantified the area of glucagon-positive cells on pancreatic sections prepared from mice treated with 4-cresol and 4-methylcatechol (Figure S10). We did not identify significant differences in α-cell density in the mouse groups. Even though other pancreatic cell types were not analyzed, these data suggest that the effects of 4-cresol on endocrine pancreatic cells involved in the regulation of glucose homeostasis may be limited to β-cells.

To investigate a possible cause of increased β-cell area and islet density induced by 4-cresol, we next used Ki67 to determine pancreatic cell proliferation in the 4 mouse groups (Figures 4A–4C). Immunohistochemistry confirmed elevated islet size 4-cresol-treated mice (153.60 ± 14.18 in CHD-fed mice; 170.00 ± 12.56 in HFD-fed mice) when compared to CHD-fed mice treated with saline (50.81 ± 2.90) (Figures 4A and 4B). The number of proliferative nuclei was increased in HFD-fed mice when compared to CHD-fed mice (Figures 4A–4C). It was also significantly increased in response to 4-cresol treatment in CHD-fed mice and remained elevated in HFD-fed mice. Increased vascularization from endothelial cells contributes to pancreatic cell proliferation and islet enlargement (Duvillié et al., 2002) and may explain the effect of 4-cresol on β-cell proliferation. To test this hypothesis, we stained pancreas sections of the 4 mouse groups with CD31, a marker of vascularization. The number of CD31⁺ cells was significantly increased in response to an HFD (Figures 4D and 4E). In both groups fed CHD or HFD, 4-cresol induced a further significant increase in CD31⁺ cells, thus demonstrating the role of this metabolite on the stimulation of pancreas vascularization.

These results illustrate the wide spectrum of pancreatic histological features and mechanisms affected by *in vivo* 4-cresol chronic administration, which may account for its effects on increased pancreas weight, enhanced glucose-stimulated insulin secretion *in vivo*, and improved glucose tolerance in a model of obesity and insulin resistance induced experimentally.
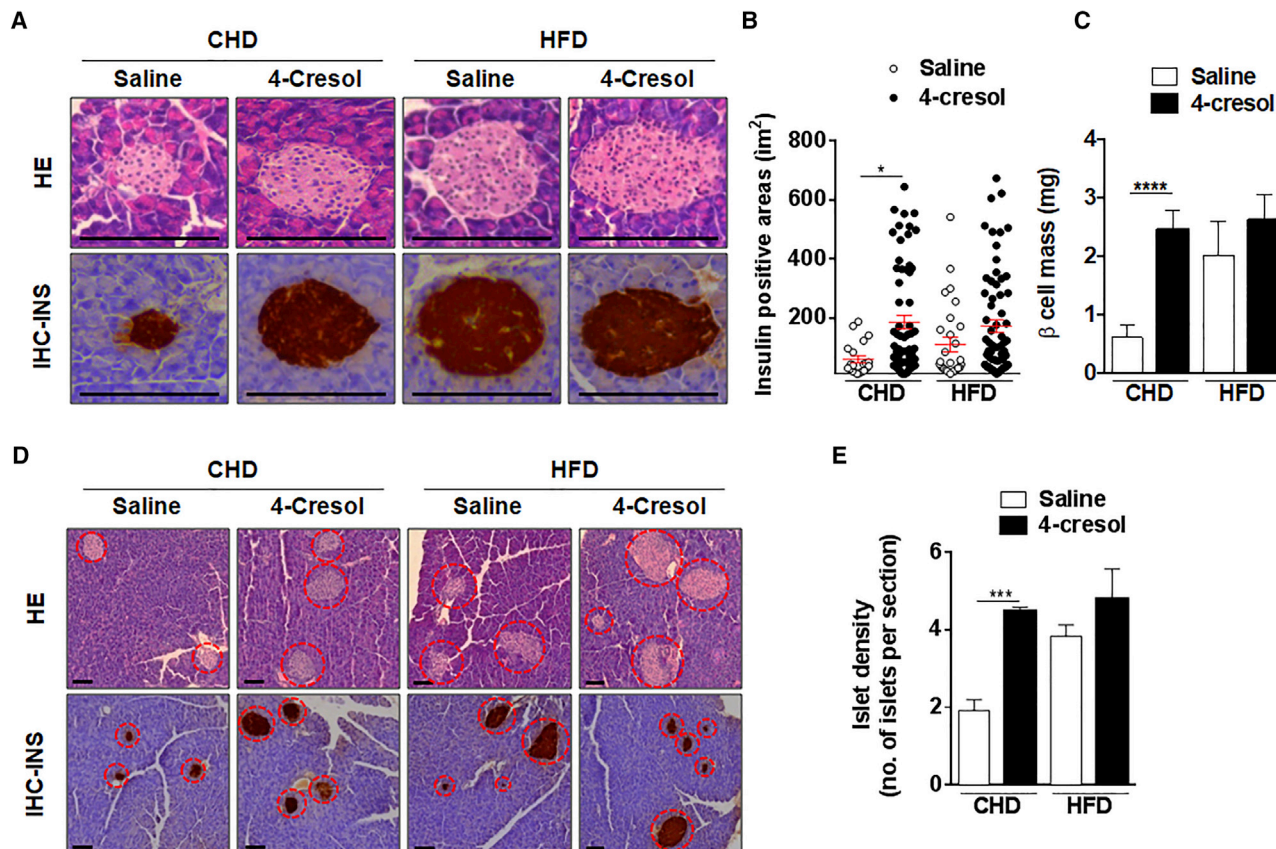
Figure 3. 4-Cresol Treatment In Vivo Increases Islet Size and Density and β-Cell Mass

(A–D) Mice were fed normal CHD or HFD and treated with chronic infusion of either 4-cresol or saline for 6 weeks. Pancreas sections were labeled with hematoxylin-eosin (H&E) and immunohistochemistry (IHC) (A) to determine insulin-positive area (B), β-cell mass (C), and islet density, as the number of islets per section (D and E).

Scale bars are 100 μm in (A) and 20 μm in (D). Each dot in (B) represents the labeled surface from a pancreas section. Results are means ± SEMs. *p < 0.05; ***p < 0.001; significantly different from relevant controls.

4-Cresol Treatment Improves Glucose Homeostasis and Boosts Insulin Secretion and Islet Density in the Goto-Kakizaki Rat

The impact of 4-cresol on enhanced insulin secretion and stimulated β-cell proliferation *in vivo* in a model of diet-induced insulin resistance and *in vitro* in isolated islets prompted us to test 4-cresol in a preclinical model of spontaneously occurring diabetes characterized by a reduction in β-cell mass. We used the Goto-Kakizaki (GK) rat, which exhibits glucose intolerance and deteriorated islet structure as a result of repeated breeding outbred Wistar rats over many generations using glucose intolerance for selecting breeders (Bihoreau et al., 2017). Chronic administration of 4-cresol had no effect on body weight (Figure S11). In contrast, the adiposity index was significantly reduced (Figure 5A), even though the GK is not considered a model of obesity. Pancreas weight nearly doubled (+94.6%, p < 0.01) in 4-cresol-treated rats (Figure 5B). This effect of 4-cresol was associated with a significant reduction in fasting glycemia (Figure 5C) and in glucose intolerance, assessed by a decrease in the glycemic response to glucose challenge throughout the IPGTT (Figure 5D) and a significant drop in cumulative glycemia

(Figures 5E and 5F). Fasting insulinemia and glucose-induced insulin secretion during the IPGTT were significantly more elevated in GK treated with 4-cresol than in rats treated with saline (Figure 5G). Pancreas histology analyses showed a significant increase in the insulin-positive area in response to 4-cresol, which was associated with increased β-cell proliferation determined by Ki67 labeling (Figures 5H–5J).

These findings strongly support data obtained in HFD-fed mice and demonstrate that 4-cresol administration dramatically improves diabetes phenotypes in a model characterized by spontaneously occurring insulin deficiency and deteriorated islet structure.

4-Cresol Stimulates Insulin Production and Glucose-Induced Insulin Secretion *In Vitro* and Increases Insulin Content in Mouse Isolated Islets

To confirm the functional role of 4-cresol in pancreatic islets, we incubated mouse islets with a concentration of 4-cresol (10 nM), which corresponds to the dose administered *in vivo* in mice. We also used 4-cresol at 100 nM to determine the maximum effective dose (ED) of this compound on islet function. The incubation
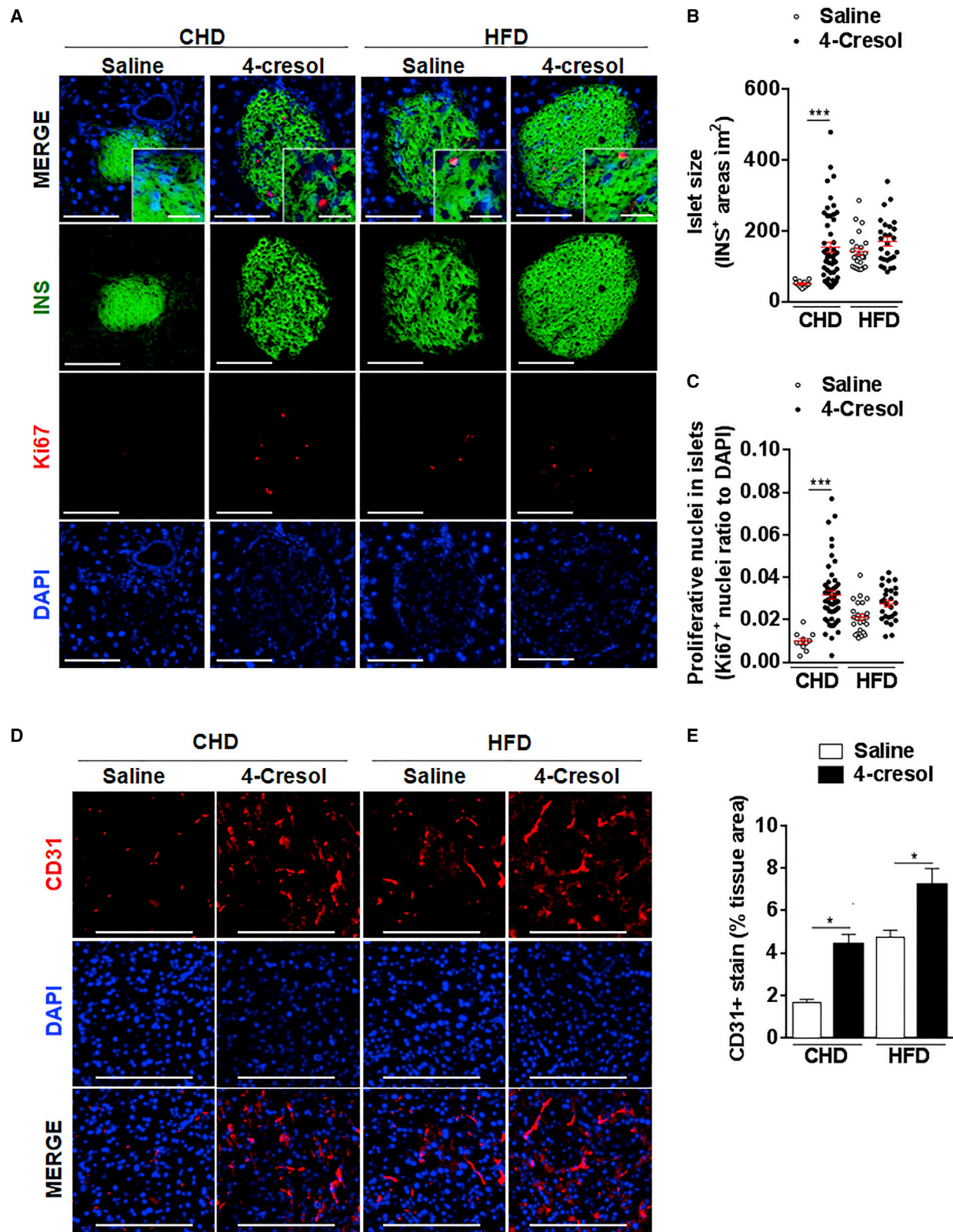
(legend on next page)

of islets with glucose 16.7 mM stimulated insulin secretion (Figure 6A). The lowest dose of 4-cresol induced an increase in insulin release under basal conditions (2.8 mM glucose) (+17.3%), a marked stimulation of insulin secretion in response to glucose 16.7 mM (+25.8%, p = 0.06) (Figure 6A), and a significant increase in islet insulin content (+33.7%, p < 0.05) (Figure 6B) when compared to islets incubated in a medium free of 4-cresol. Incubation with 4-cresol at 100 nM had no effect on insulin production, secretion, and content when compared to controls.

4-Cresol Stimulates β-Cell Proliferation in Mouse Isolated Islets

We next assessed the effect of 4-cresol on β-cell proliferation *in vitro*, which we compared to that of the incretin hormone glucagon-like peptide-1 (GLP-1), a well-established therapeutic target in diabetes (Capozzi et al., 2018; Tudurí et al., 2016) that promotes pancreatic cell proliferation and β-cell neogenesis (Brubaker and Drucker, 2004; Cornu et al., 2010). Fewer than 1% of islet cells showed Ki67 staining after 48 h of culture in control conditions in the absence of stimulation with 4-cresol or GLP-1. Treatment of mouse isolated islets with 4-cresol 10 nM for 48 h induced a strong and significant increase (+138%; p < 0.05) in the percentage of Ki67$^+$ nuclei when compared to control islets, indicating increased β-cell proliferation in response to 4-cresol, whereas incubation with the higher concentration of 4-cresol (100 nM) induced a non-significant stimulatory effect (+61%) (Figures 6C, 6E, and S12). The ED of GLP-1 (10 nM) induced a significant increase in β-cell proliferation (+178%; p < 0.05) of a magnitude similar to that induced by 4-cresol 10 nM, whereas the median ED (ED$_{50}$) of GLP-1 (1 nM) resulted in a non-significant stimulatory effect (+50%) (Figures 6D, 6E, and S12). These *in vitro* data in isolated islets corroborate the capacity of β-cells to proliferate in response to 4-cresol, as observed *in vivo* in mice and rats treated chronically with 4-cresol. They indicate that 4-cresol and GLP-1 at the same concentration have the same efficacy to stimulate β-cell proliferation.

Chronic 4-Cresol Treatment Is Associated with Profound Changes in Pancreas Gene Expression

To gain insights into molecular mechanisms that contribute to structural and functional changes induced by 4-cresol in the pancreas *in vivo*, the expression of selected genes covering various aspects of pancreas biology was tested by qRT-PCR in HFD-fed and control mice (Figure 7A) and in GK rats (Figure 7B). The expression of uncoupling protein 2 (*Ucp2*), interleukins (*Il6*, *Il10*), and tumor necrosis factor (*Tnfa*) was increased by HFD feeding. Chronic treatment by 4-cresol in CHD-fed mice led to the increased transcription of genes encoding amylase, vascular endothelial growth factor (*Vegf*), brain-derived neurotrophic factor (*Bdnf*), *Il10*, and *Sirt1* when compared to saline-

treated CHD-fed mice. Stimulated transcription of *Sirt1* was associated with an increased NAD:NADH ratio, which is known to regulate SIRT1 activity (Cantó et al., 2009). Enhanced expression of the insulin gene (*Ins1*) and the transcription factor HNF1 homeobox A (*Hnf1α*) by 4-cresol and reduced expression of *Ucp2* in this comparison were not statistically significant. In mice fed an HFD, 4-cresol induced a significant overexpression of genes encoding *Sirt1* and *Ins1* and significantly reduced the expression of *Ucp2*, *Il6*, and *Tnfa* when compared to HFD-fed mice treated with saline. The *Il10* transcript level remained elevated in HFD-fed mice treated with 4-cresol. *Bndf*, *Hnf1α*, and *Vegf* were also strongly overexpressed in response to 4-cresol in these mice. The stimulatory effects of the chronic administration of 4-cresol on the expression of *Sirt1*, *Ins1*, *Hnf1α*, *Il10*, and *Vegfa* were replicated in the GK pancreas (Figure 7B). The expression of amylase, *Il6*, and *Tnfa* was strongly altered in 4-cresol-treated GK rats.

Due to the strong similarities in the biological effects of 4-cresol and harmine, an inhibitor of the dual specificity tyrosine phosphorylation regulated kinase (DYRK1A) known to stimulate β-cell proliferation (Dirice et al., 2016; Shen et al., 2015), we tested the expression of this gene in the pancreas of fat-fed mice and GK rats treated with 4-cresol, as well as in mouse isolated islets incubated with 10 nM cresol (Figure 7C). In both *in vivo* models and in isolated islets, 4-cresol consistently downregulated the pancreatic expression of DYRK1A, thus suggesting that 4-cresol affects signaling pathways similar to those mediating the cellular action of other natural products, such as harmine.

These results demonstrate the wide-ranging molecular consequences of 4-cresol treatment in the pancreas of animal models of diabetes-induced experimentally by dietary changes or caused by naturally occurring genetic polymorphisms and provide insights into possible mediating mechanisms.

DISCUSSION

We report correlations between T2D and variations in the serum concentrations of a series of metabolites derived by GC-MS-based metabolomics. Significant associations were found with metabolites, including 4-cresol, which was tested for its biological role *in vivo* in preclinical models of spontaneous or experimentally induced diabetes and *in vitro* in β-cells. We demonstrate that chronic administration of a non-toxic dose of 4-cresol improves glycemic control, enhances glucose-stimulated insulin secretion, reduces adiposity and liver triglycerides, and stimulates pancreatic islet density, vascularization, and β-cell proliferation *in vivo* and *in vitro*. *In vivo* insulin sensitivity was not affected by 4-cresol treatment. These effects mimic metabolic improvements induced by harmine and may be mediated in part through the downregulated expression of DYRK1A.

Figure 4. Chronic Treatment of Mice by 4-Cresol Promotes β-Cell Proliferation and Vascularization

Mice were fed normal chow diet (CHD) or high fat diet (HFD) and treated with chronic infusion of either 4-cresol or saline for 6 weeks. Pancreas sections were treated with primary anti-Ki67 antibody and DAPI to stain (A) and quantify islet size (B) and proliferative nuclei (C), and with anti-CD31 antibody and DAPI to stain (D) and quantify (E) endothelial cells.

Scale bars are 100 μm. Each dot in (B), (C), and (E) represents data from a pancreas section. Results are means ±SEMs. *p < 0.05; ***p < 0.001; significantly different from relevant controls.
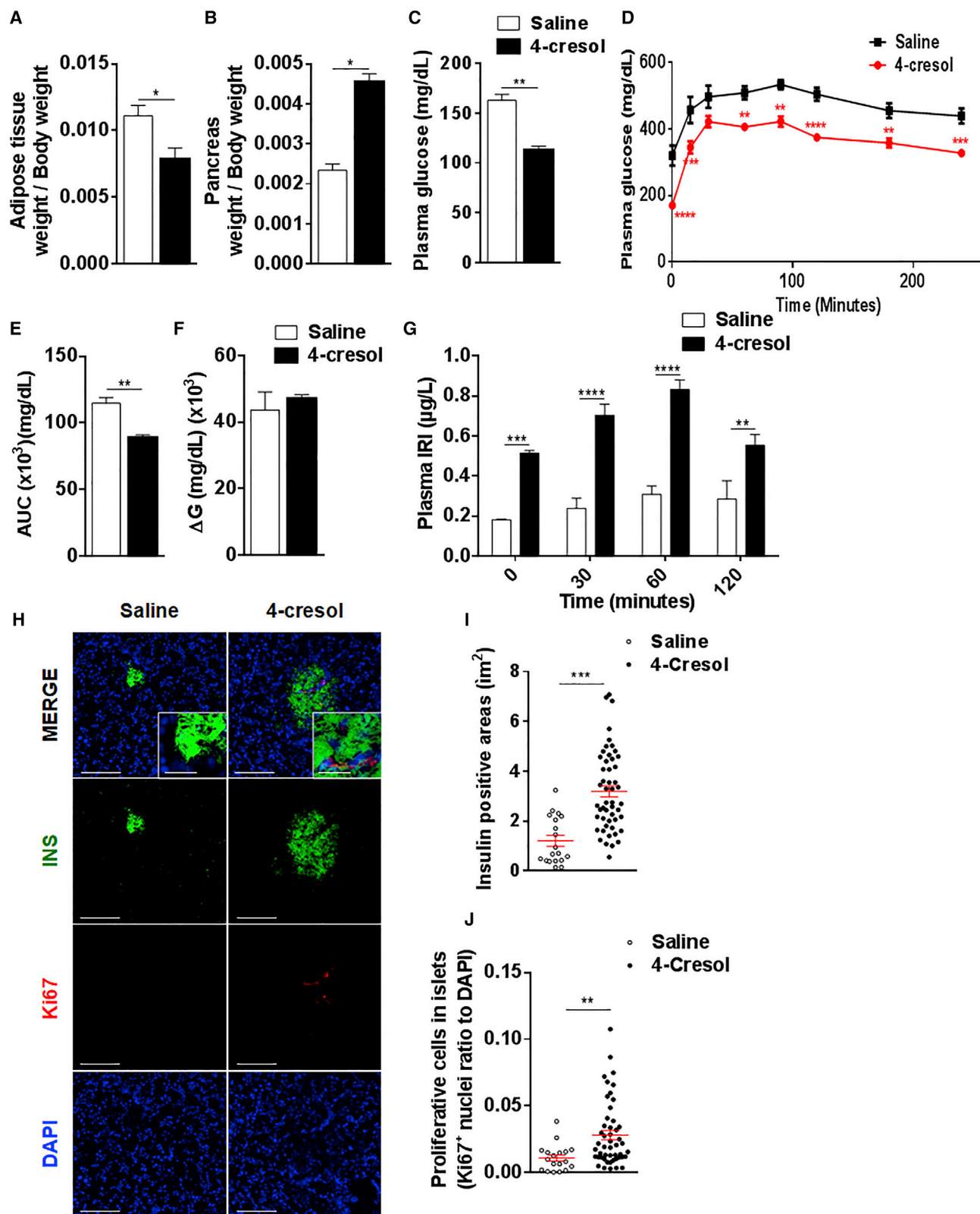
(legend on next page)

Our metabolomic approach identified systematic correlations between T2D and a metabotype (Gavaghan et al., 2000) of 6 co-associated metabolites, which covers obvious candidates for this condition, including, for example, glucose, branched-chain amino acids, and mannose, which is proposed as an accurate marker of insulin resistance (Lee et al., 2016). Glucose- and mannose-mediated inhibition of the cellular uptake of 1,5-anhydro-D-sorbitol (Saito et al., 1996), a marker of short-term glycemic control (Dungan, 2008), supports the strongly significant negative correlation between serum 1,5-anhydro-D-sorbitol and T2D in our study. Other metabolites showing a marginal correlation with T2D includes 2-hydroxybutyric acid, which is elevated in the plasma of T2D patients (Li et al., 2009) and could be a predictive marker of insulin resistance (Gall et al., 2010), and 2-amino adipic acid, which is associated with T2D risk (Wang et al., 2013). Stimulation of insulin secretion in vitro (Wang et al., 2013) by 2-amino adipic acid and its regulation by the dehydrogenase E1 and transketolase domain-containing 1 gene (DHTKD1), which plays critical roles in diabetes pathogenesis (Wu et al., 2014) and in mitochondrial energy production and biogenesis (Xu et al., 2013), suggest wide-ranging roles for 2-amino adipic acid in the pathogenesis of metabolic disorders.

4-Cresol is a potential end product of protein breakdown by mammalian organisms and a xenobiotic substance. It is naturally present in food (smoked foods, tomatoes, asparagus, dairy products), drinks (coffee, black tea, wine), cigarette smoke, wood burning, and surface waters and groundwater (https://www.atsdr.cdc.gov/), and can be synthesized from phenol found in the environment and absorbed by ingestion, inhalation, or dermal contact. Lethal dose (LD_{50}) for 4-cresol given orally ranges from 200 to 5,000 mg/kg/day (Andersen, 2006). Irritation to the respiratory epithelium and deteriorated liver function can be caused by dietary exposure to doses of 4-cresol (240–2,000 mg/kg/day), which are much higher than those used in our in vivo (0.5 mg/kg/day) and in vitro (10 nM) studies. 4-Cresol is also a product of the colonic fermentation of tyrosine and phenylalanine (Cummings, 1983), and variations in circulating 4-cresol in the host organism may reflect architectural alterations of the gut microbiota that have been consistently reported in obese and diabetic patients (Hansen et al., 2015; Pedersen et al., 2016; Qin et al., 2012). This concept of microbiome-host genome crosstalk is supported by instances of associations between cardiometabolic diseases and microbial-mammalian co-metabolites (e.g., hippurate, methylamines, short-chain fatty acids) (Brial et al., 2018) that metabolomic technologies can detect and quantify in biological matrices.

Beneficial effects of the chronic administration of low dose of 4-cresol in vivo in fat-fed mice and in GK rats validate the inverse correlation of this metabolite with T2D in humans in our study.

Deeper analyses in these models underline the wide-ranging impact of 4-cresol on improved glucose regulation, enhanced insulinemia, insulin secretion induced by glucose in vivo, insulin content in vitro, islet expansion and β-cell proliferation, increased pancreas weight, which undoubtedly affects acinar cells possibly through a local effect of stimulated insulin release, and reduced adiposity, liver triglycerides, and food intake in response to fat feeding. In line with our in vivo findings, 4-cresol was shown to inhibit the proliferation and differentiation of 3T3-L1 preadipocytes (Tanaka et al., 2014). This is consistent with the report of a negative association between body mass index and urine concentration of its detoxification product 4-cresyl sulfate in humans (Elliott et al., 2015), which underlines the importance of the cresol pathway in cardiometabolic diseases. Conserved effects of 4-cresol and 4-MC, one of its potential products through dehydrogenation by bacterial metabolism (Kolomytseva et al., 2007), on glucose tolerance, insulin secretion, adiposity, and body and organ weights support this hypothesis and suggest a low specificity of 4-cresol and 4-MC, which may regulate similar signaling systems. This is further supported by the reduction of β-cell apoptosis and hyperglycemia mediated by 4-MC in diabetic rats (Gezginci-Oktayoglu and Bolkent, 2011).

In addition, the results from pancreas histopathology and gene expression analysis in both preclinical models suggest that 4-cresol contributes to the reduction in inflammation through the downregulated expression of Il6 and Tnfa and the stimulated expression of Il10, an anti-inflammatory marker involved in vascularization and resistance to apoptosis (Hatanaka et al., 2001; Zeng et al., 2010). Upregulated expression of Vegf and Bdnf suggests enhanced vascularization and parasympathetic tone, respectively. Of note, Bdnf reduces hyperglycemia and increases the number and area of pancreatic islets in diabetic db/db mice (Yamanaka et al., 2006).

The upregulated pancreatic expression of Sirt1 by 4-cresol in mice and GK rats along with an increased NAD^+:NADH ratio, which enhances SIRT1 activity (Cantó et al., 2009), and the downregulated expression of Ucp2 in mice suggest that it may mediate the effects of 4-cresol. SIRT1 stimulates insulin secretion and lipolysis; reduces adipogenesis, liver lipid accumulation, and inflammation; and improves glucose homeostasis (Liang et al., 2009). SIRT1 is regulated by the polyphenol resveratrol, which reduces adiposity through the stimulation of lipolysis and the inhibition of lipogenesis, exhibits anti-inflammatory effects through the downregulated expression of Tnfa and Il6 (Baile et al., 2011), and potentiates insulin secretion in insulinoma cells and human islets (Vetterli et al., 2011). These data suggest convergent biological roles of natural products or polyphenols and the phenol derivative 4-cresol, which may share ligands

Figure 5. 4-Cresol Treatment *In Vivo* in Goto-Kakizaki Rats Improves Glucose Homeostasis and Boosts Insulin Secretion and Islet Density
(A–J) Adipose tissue and pancreas weight (A and B), fasting glycemia (C), glucose tolerance profile (D) and indices (E–F), glucose-stimulated insulin secretion (G), pancreas histopathology (H) and quantitative analysisi of insulin positive area (I) and islet cells proliferation (J) were determined in rats of the Goto-Kakizaki (GK) model of T2D chronically treated with 4-cresol (n = 6) or with saline (n = 5) for 6 weeks. Pancreas sections were labeled either with H&E and IHC to determine the insulin-positive area (I) and treated with Ki67 and DAPI to stain and quantify proliferative nuclei (J).
Scale bars are 100 μm in (H). Each dot in (I) represents the insulin-labeled surface from a pancreas section. AUC was calculated as the sum of plasma glucose values during the IPGTT. ΔG is the AUC over the baseline value integrated over the 240 min of the test. Data were analyzed using the unpaired Mann-Whitney test. Results are means ± SEMs. **p < 0.01; ***p < 0.001; ****p < 0.0001; significantly different from GK rats treated with saline. IRI, immunoreactive insulin.
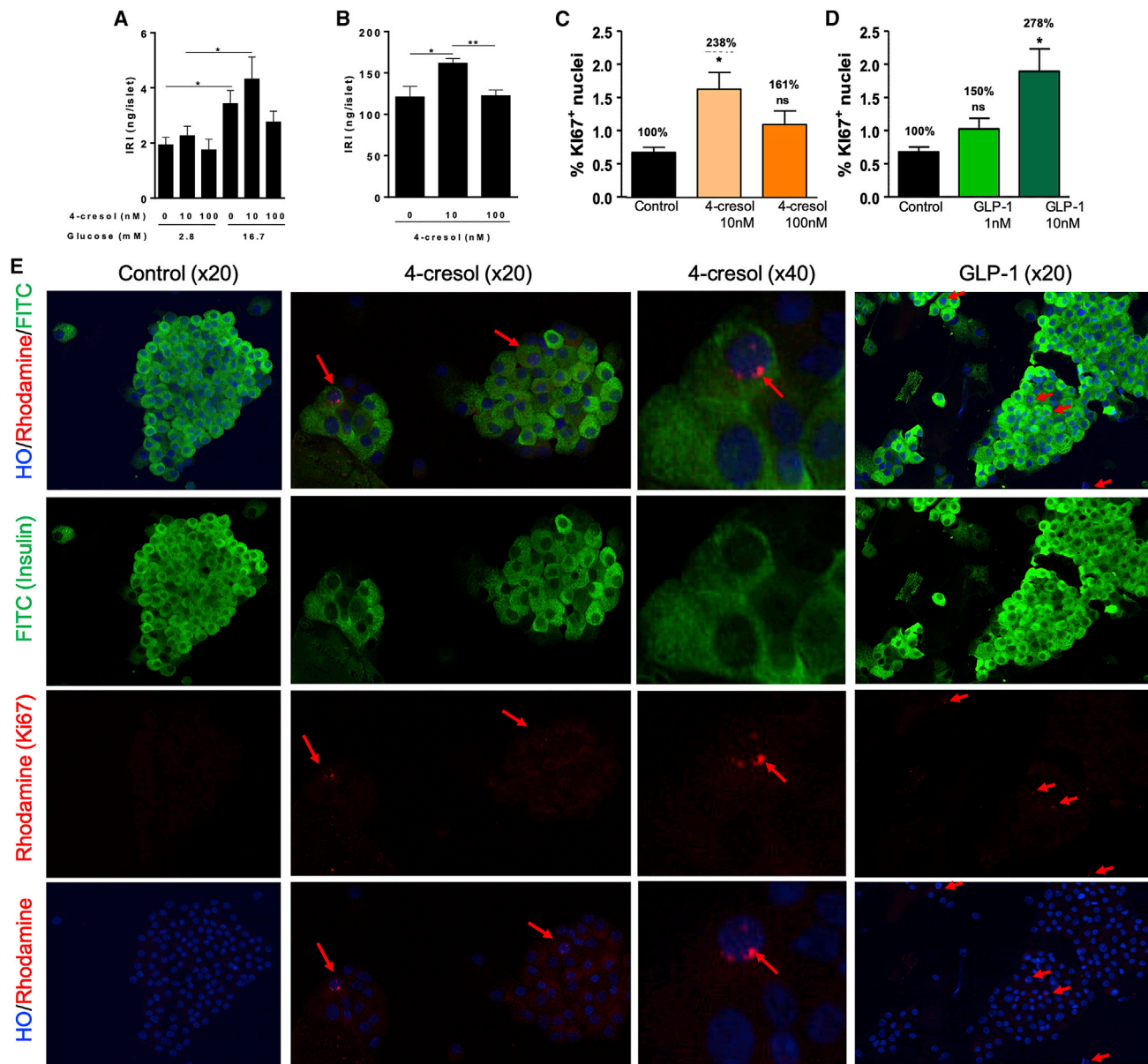
Figure 6. 4-Cresol Stimulates Insulin Content and β-Cell Proliferation In Vitro in Isolated Islets

(A and B) Insulin release and secretion in response to glucose (A) and insulin content (B) were determined in isolated mouse islets incubated with a control medium and with solutions of 4-cresol 10 or 100 nM.

(C and D) β-Cell proliferation was determined in the presence of 4-cresol (10 and 100 nM) (C) or GLP-1 at its known effective dose (10 nM) or median effective dose (1 nM) (D).

(E) Typical examples of Ki67 labeling of β-cell proliferative nuclei in islets treated with 4-cresol 10 nM or GLP-1 10 nM and in control islets treated with a medium free of 4-cresol and GLP-1 are shown.

β-Cell proliferation quantitative analyses were performed in 160 control islets and in 120 islets incubated with 4-cresol or GLP-1. A minimum of 6,000 cells per treatment in randomly selected fields were counted. Scale bars are 40 μm. IRI, immunoreactive insulin. Results were expressed as means ± SEMs. **p < 0.01, *p < 0.05 significantly different between treated islets and controls.

and signaling mechanisms leading to improved glucose homeostasis. We showed that 4-cresol and harmine exhibit very similar effects on increased islet mass and improved glucose regulation (Wang et al., 2015). Harmine inhibits the kinase DYRK1A, resulting in increased β-cell proliferation and islet mass (Wang et al., 2015). There is compelling evidence supporting causal relations between DYRK1a inhibition and the induction of β-cell proliferation, the stimulation of glucose-induced insulin secretion, and the increase in β-cell mass and insulin content (Dirice et al., 2016; Shen et al., 2015; Wang et al., 2019). The impact of
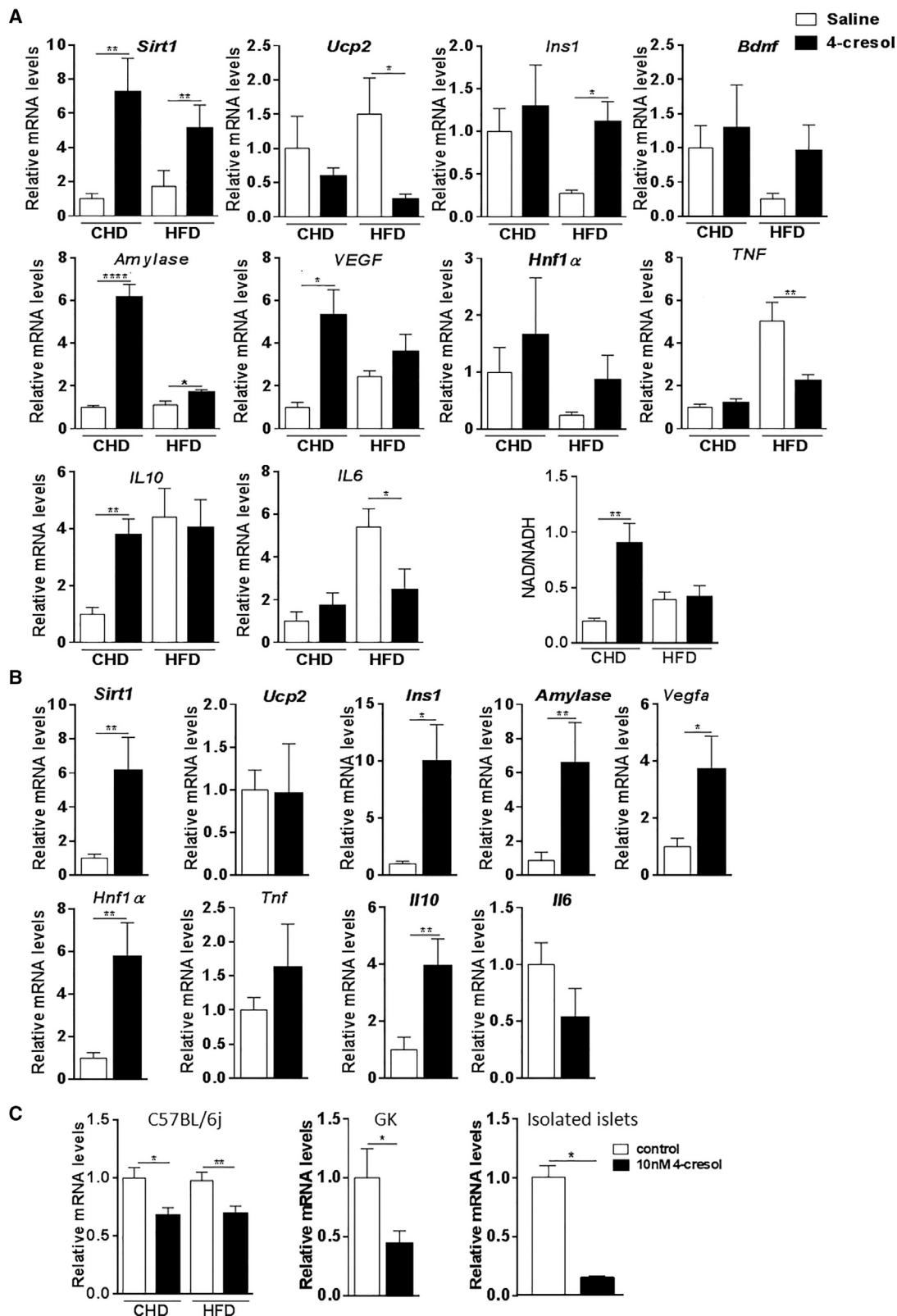
(legend on next page)

polyphenols on DYRK1a inhibition is suggested by the rescue of neurobehavioral deficits in transgenic mice overexpressing DYRK1a through treatment with green tea polyphenols (Guedj et al., 2009). Our results indicate that the mechanisms mediating the effects of 4-cresol on improved β-cell function involve at least in part the inhibition of DYRK1A expression and support the emerging role of kinases in the cellular function of microbial metabolites (Zhou et al., 2018).

In conclusion, our findings illustrate the power of systematic metabolic profiling to identify metabolites involved in chronic diseases through the demonstration of the beneficial role of low doses of 4-cresol on β-cell function and cardiometabolic endophenotypes. Deeper exploitation of the metabolomic dataset beyond targeted analysis of known molecules may uncover networks of metabolites that are co-regulated with 4-cresol and point to underlying gene pathways. The similar magnitude of β-cell proliferation capacity by 4-cresol and GLP-1 in our study emphasizes the value of 4-cresol and its co-metabolites as therapeutic targets in syndromes characterized by reduced β-cell mass and insulin deficiency. Therapeutic exploitation of bacterial ecosystems that synthesize 4-cresol (Saito et al., 2018) is an important objective for future investigations, which may have important relevance in the treatment of T2D. Of note, recent analyses of gut metagenome sequencing and metabolome profiling indicate that blood p-cresol sulfate is positively correlated with microbiome diversity (Pallister et al., 2017), suggesting a reduced risk of cardiometabolic diseases (Le Chatelier et al., 2013). Our results pave the way to the identification of diagnostic and prognostic metabolic biomarkers at the crossroads between diabetes risk and microbiome architecture and activity that can provide therapeutic solutions in diabetes.

STAR★METHODS

Detailed methods are provided in the online version of this paper and include the following:

- KEY RESOURCES TABLE
- LEAD CONTACT AND MATERIALS AVAILABILITY
- EXPERIMENTAL MODEL AND SUBJECT DETAILS
  - ○ Study Subjects
  - ○ Animals
- METHOD DETAILS
  - ○ Chemicals
  - ○ Human serum sample preparation
  - ○ Gas chromatography coupled to mass spectrometry (GC-MS)
  - ○ Targeted metabolomic data analysis
  - ○ Animal experiments
  - ○ Histology and immunohistochemistry of animal tissues
  - ○ *In vitro* insulin secretion in mouse isolated islets
  - ○ Analysis of β-cell proliferation *in vitro* in mouse isolated islets
  - ○ RNA isolation and quantitative RT-PCR
- QUANTIFICATION AND STATISTICAL ANALYSIS
  - ○ Analytical assays
  - ○ Statistical analyses
- DATA AND CODE AVAILABILITY

AUTHOR CONTRIBUTIONS

P.Z., F.M., M.L., M.-E.D., and D.G. conceived the study. P.Z. provided patients' serum samples. K.S., T.-A.S., and F.M. carried out targeted GC-MS metabolomic analyses. F.B., A.L.L., and N.P. carried out the mouse experiments. F.B., K.M., and C.M. incubated isolated islets. F.B., A.L.L., and F.A. performed the histology and gene expression analyses. Y.K. and L.H. performed the statistical analyses. P.Z. and D.G. wrote the manuscript. All of the authors have given approval to the final version of the manuscript.

DECLARATION OF INTERESTS

REFERENCES

Andersen, A. (2006). Final report on the safety assessment of sodium p-chloro-m-cresol, p-chloro-m-cresol, chlorothymol, mixed cresols, m-cresol, o-cresol, p-cresol, isopropyl cresols, thymol, o-cymen-5-ol, and carvacrol. Int. J. Toxicol. *25 (Suppl 1)*, 29–127.

Baile, C.A., Yang, J.Y., Rayalam, S., Hartzell, D.L., Lai, C.Y., Andersen, C., and Della-Fera, M.A. (2011). Effect of resveratrol on fat mobilization. Ann. N Y Acad. Sci. *1215*, 40–47.

Figure 7. Effects of Chronic Administration of 4-Cresol on Gene Expression in Pancreas and Isolated Islets
(A and B) Gene transcription was determined by qRT-PCR in total pancreas of C57BL/6J mice fed control CHD or HFD (A) and Goto-Kakizaki (GK) rats (B) treated chronically with 4-cresol and in mouse islets incubated with 10 nM 4-cresol. The level of NAD and NADH was measured in total mouse pancreas.
(C) Expression of *Dyrk1a* was determined in total pancreas of C57BL/6J mice and GK rats treated chronically with 4-cresol and in mouse isolated islets incubated with 10 nM cresol.
All of the experiments were carried out in 6 biological replicates per group. Results are means ± SEMs. *p < 0.05; **p < 0.01; ****p < 0.0001; significantly different from relevant controls.

Barouki, R., Audouze, K., Coumoul, X., Demenais, F., and Gauguier, D. (2018). Integration of the human exposome with the human genome to advance medicine. Biochimie 152, 155–158.

Barroso, I., and McCarthy, M.I. (2019). The Genetic Basis of Metabolic Disease. Cell 177, 146–161.

Becker, W., Weber, Y., Wetzel, K., Eirmbter, K., Tejedor, F.J., and Joost, H.G. (1998). Sequence characteristics, subcellular localization, and substrate specificity of DYRK-related kinases, a novel family of dual specificity protein kinases. J. Biol. Chem. 273, 25893–25902.

Bihoreau, M.T., Dumas, M.E., Lathrop, M., and Gauguier, D. (2017). Genomic regulation of type 2 diabetes endophenotypes: Contribution from genetic studies in the Goto-Kakizaki rat. Biochimie 143, 56–65.

Brial, F., Le Lay, A., Dumas, M.E., and Gauguier, D. (2018). Implication of gut microbiota metabolites in cardiovascular and metabolic diseases. Cell. Mol. Life Sci. 75, 3977–3990.

Brindle, J.T., Antti, H., Holmes, E., Tranter, G., Nicholson, J.K., Bethell, H.W., Clarke, S., Schofield, P.M., McKilligin, E., Mosedale, D.E., and Grainger, D.J. (2002). Rapid and noninvasive diagnosis of the presence and severity of coronary heart disease using 1H-NMR-based metabonomics. Nat. Med. 8, 1439–1444.

Brubaker, P.L., and Drucker, D.J. (2004). Minireview: glucagon-like peptides regulate cell proliferation and apoptosis in the pancreas, gut, and central nervous system. Endocrinology 145, 2653–2659.

Cantó, C., Gerhart-Hines, Z., Feige, J.N., Lagouge, M., Noriega, L., Milne, J.C., Elliott, P.J., Puigserver, P., and Auwerx, J. (2009). AMPK regulates energy expenditure by modulating NAD+ metabolism and SIRT1 activity. Nature 458, 1056–1060.

Capozzi, M.E., DiMarchi, R.D., Tschöp, M.H., Finan, B., and Campbell, J.E. (2018). Targeting the Incretin/Glucagon System With Triagonists to Treat Diabetes. Endocr. Rev. 39, 719–738.

Cornu, M., Modi, H., Kawamori, D., Kulkarni, R.N., Joffraud, M., and Thorens, B. (2010). Glucagon-like peptide-1 increases beta-cell glucose competence and proliferation by translational induction of insulin-like growth factor-1 receptor expression. J. Biol. Chem. 285, 10538–10545.

Cummings, J.H. (1983). Fermentation in the human large intestine: evidence and implications for health. Lancet 1, 1206–1209.

Dirice, E., Walpita, D., Vetere, A., Meier, B.C., Kahraman, S., Hu, J., Dančík, V., Burns, S.M., Gilbert, T.J., Olson, D.E., et al. (2016). Inhibition of DYRK1A Stimulates Human β-Cell Proliferation. Diabetes 65, 1660–1671.

Dumas, M.E., Barton, R.H., Toye, A., Cloarec, O., Blancher, C., Rothwell, A., Fearnside, J., Tatoud, R., Blanc, V., Lindon, J.C., et al. (2006). Metabolic profiling reveals a contribution of gut microbiota to fatty liver phenotype in insulin-resistant mice. Proc. Natl. Acad. Sci. USA 103, 12511–12516.

Dungan, K.M. (2008). 1,5-anhydroglucitol (GlycoMark) as a marker of short-term glycemic control and glycemic excursions. Expert Rev. Mol. Diagn. 8, 9–19.

Duvillié, B., Currie, C., Chrones, T., Bucchini, D., Jami, J., Joshi, R.L., and Hill, D.J. (2002). Increased islet cell proliferation, decreased apoptosis, and greater vascularization leading to beta-cell hyperplasia in mutant mice lacking insulin. Endocrinology 143, 1530–1537.

Elliott, P., Posma, J.M., Chan, Q., Garcia-Perez, I., Wijeyesekera, A., Bictash, M., Ebbels, T.M., Ueshima, H., Zhao, L., van Horn, L., et al. (2015). Urinary metabolic signatures of human adiposity. Sci. Transl. Med. 7, 285ra62.

Franks, P.W., and McCarthy, M.I. (2016). Exposing the exposures responsible for type 2 diabetes and obesity. Science 354, 69–73.

Gall, W.E., Beebe, K., Lawton, K.A., Adam, K.P., Mitchell, M.W., Nakhle, P.J., Ryals, J.A., Milburn, M.V., Nannipieri, M., Camastra, S., et al.; RISC Study Group (2010). alpha-hydroxybutyrate is an early biomarker of insulin resistance and glucose intolerance in a nondiabetic population. PLoS One 5, e10883.

Gavaghan, C.L., Holmes, E., Lenz, E., Wilson, I.D., and Nicholson, J.K. (2000). An NMR-based metabonomic approach to investigate the biochemical conse-

quences of genetic strain differences: application to the C57BL10J and Alpk:ApfCD mouse. FEBS Lett. 484, 169–174.

Gezginci-Oktayoglu, S., and Bolkent, S. (2011). 4-Methlycatechol prevents NGF/p75(NTR)-mediated apoptosis via NGF/TrkA system in pancreatic β cells. Neuropeptides 45, 143–150.

Golson, M.L., Bush, W.S., and Brissova, M. (2014). Automated quantification of pancreatic β-cell mass. Am. J. Physiol. Endocrinol. Metab. 306, E1460–E1467.

Guedj, F., Sébrié, C., Rivals, I., Ledru, A., Paly, E., Bizot, J.C., Smith, D., Rubin, E., Gillet, B., Arbones, M., and Delabar, J.M. (2009). Green tea polyphenols rescue of brain defects induced by overexpression of DYRK1A. PLoS One 4, e4606.

Hansen, T.H., Gøbel, R.J., Hansen, T., and Pedersen, O. (2015). The gut microbiome in cardio-metabolic health. Genome Med. 7, 33.

Hatanaka, H., Abe, Y., Naruke, M., Tokunaga, T., Oshika, Y., Kawakami, T., Osada, H., Nagata, J., Kamochi, J., Tsuchida, T., et al. (2001). Significant correlation between interleukin 10 expression and vascularization through angiopoietin/TIE2 networks in non-small cell lung cancer. Clin. Cancer Res. 7, 1287–1292.

Kirschenlohr, H.L., Griffin, J.L., Clarke, S.C., Rhydwen, R., Grace, A.A., Schofield, P.M., Brindle, K.M., and Metcalfe, J.C. (2006). Proton NMR analysis of plasma is a weak predictor of coronary artery disease. Nat. Med. 12, 705–710.

Kolomytseva, M.P., Baskunov, B.P., and Golovleva, L.A. (2007). Intradiol pathway of para-cresol conversion by Rhodococcus opacus 1CP. Biotechnol. J. 2, 886–893.

Le Chatelier, E., Nielsen, T., Qin, J., Prifti, E., Hildebrand, F., Falony, G., Almeida, M., Arumugam, M., Batto, J.M., Kennedy, S., et al.; MetaHIT consortium (2013). Richness of human gut microbiome correlates with metabolic markers. Nature 500, 541–546.

Lee, S., Zhang, C., Kilicarslan, M., Piening, B.D., Bjornson, E., Hallström, B.M., Groen, A.K., Ferrannini, E., Laakso, M., Snyder, M., et al. (2016). Integrated Network Analysis Reveals an Association between Plasma Mannose Levels and Insulin Resistance. Cell Metab. 24, 172–184.

Li, X., Xu, Z., Lu, X., Yang, X., Yin, P., Kong, H., Yu, Y., and Xu, G. (2009). Comprehensive two-dimensional gas chromatography/time-of-flight mass spectrometry for metabonomics: Biomarker discovery for diabetes mellitus. Anal. Chim. Acta 633, 257–262.

Liang, F., Kume, S., and Koya, D. (2009). SIRT1 and insulin resistance. Nat. Rev. Endocrinol. 5, 367–373.

Livak, K.J., and Schmittgen, T.D. (2001). Analysis of relative gene expression data using real-time quantitative PCR and the 2(-Delta Delta C(T)) Method. Methods 25, 402–408.

Nicholson, J.K., Connelly, J., Lindon, J.C., and Holmes, E. (2002). Metabonomics: a platform for studying drug toxicity and gene function. Nat. Rev. Drug Discov. 1, 153–161.

Pallister, T., Jackson, M.A., Martin, T.C., Zierer, J., Jennings, A., Mohney, R.P., MacGregor, A., Steves, C.J., Cassidy, A., Spector, T.D., and Menni, C. (2017). Hippurate as a metabolomic marker of gut microbiome diversity: Modulation by diet and relationship to metabolic syndrome. Sci. Rep. 7, 13670.

Pedersen, H.K., Gudmundsdottir, V., Nielsen, H.B., Hyotylainen, T., Nielsen, T., Jensen, B.A., Forslund, K., Hildebrand, F., Prifti, E., Falony, G., et al.; MetaHIT Consortium (2016). Human gut microbes impact host serum metabolome and insulin sensitivity. Nature 535, 376–381.

Qin, J., Li, Y., Cai, Z., Li, S., Zhu, J., Zhang, F., Liang, S., Zhang, W., Guan, Y., Shen, D., et al. (2012). A metagenome-wide association study of gut microbiota in type 2 diabetes. Nature 490, 55–60.

Saade, S., Cazier, J.B., Ghassibe-Sabbagh, M., Youhanna, S., Badro, D.A., Kamatani, Y., Hager, J., Yeretzian, J.S., El-Khazen, G., Haber, M., et al.; FGENTCARD consortium (2011). Large scale association analysis identifies three susceptibility loci for coronary artery disease. PLoS One 6, e29427.

Saito, H., Ohtomo, T., and Inui, K. (1996). Na(+)-dependent uptake of 1,5-anhydro-D-glucitol via the transport systems for D-glucose and D-mannose in the kidney epithelial cell line, LLC-PK1. Nippon Jinzo Gakkai Shi 38, 435–440.

Saito, Y., Sato, T., Nomoto, K., and Tsuji, H. (2018). Identification of phenol- and p-cresol-producing intestinal bacteria by using media supplemented with tyrosine and its metabolites. FEMS Microbiol. Ecol. 94, fiy125.

Shen, W., Taylor, B., Jin, Q., Nguyen-Tran, V., Meeusen, S., Zhang, Y.Q., Kamireddy, A., Swafford, A., Powers, A.F., Walker, J., et al. (2015). Inhibition of DYRK1A and GSK3B induces human β-cell proliferation. Nat. Commun. 6, 8372.

Srour, B., Fezeu, L.K., Kesse-Guyot, E., Allès, B., Méjean, C., Andrianasolo, R.M., Chazelas, E., Deschasaux, M., Hercberg, S., Galan, P., et al. (2019). Ultra-processed food intake and risk of cardiovascular disease: prospective cohort study (NutriNet-Santé). BMJ 365, l1451.

Tanaka, S., Yano, S., Sheikh, A.M., Nagai, A., and Sugimoto, T. (2014). Effects of uremic toxin p-cresol on proliferation, apoptosis, differentiation, and glucose uptake in 3T3-L1 cells. Artif. Organs 38, 566–571.

Tudurí, E., López, M., Diéguez, C., Nadal, A., and Nogueiras, R. (2016). Glucagon-Like Peptide 1 Analogs and their Effects on Pancreatic Islets. Trends Endocrinol. Metab. 27, 304–318.

Vetterli, L., Brun, T., Giovannoni, L., Bosco, D., and Maechler, P. (2011). Resveratrol potentiates glucose-stimulated insulin secretion in INS-1E beta-cells and human islets through a SIRT1-dependent mechanism. J. Biol. Chem. 286, 6049–6060.

Wang, T.J., Ngo, D., Psychogios, N., Dejam, A., Larson, M.G., Vasan, R.S., Ghorbani, A., O'Sullivan, J., Cheng, S., Rhee, E.P., et al. (2013). 2-Aminoadipic acid is a biomarker for diabetes risk. J. Clin. Invest. 123, 4309–4317.

Wang, P., Alvarez-Perez, J.C., Felsenfeld, D.P., Liu, H., Sivendran, S., Bender, A., Kumar, A., Sanchez, R., Scott, D.K., Garcia-Ocaña, A., and Stewart, A.F. (2015). A high-throughput chemical screen reveals that harmine-mediated in-hibition of DYRK1A increases human pancreatic beta cell replication. Nat. Med. 21, 383–388.

Wang, P., Karakose, E., Liu, H., Swartz, E., Ackeifi, C., Zlatanic, V., Wilson, J., González, B.J., Bender, A., Takane, K.K., et al. (2019). Combined Inhibition of DYRK1A, SMAD, and Trithorax Pathways Synergizes to Induce Robust Replication in Adult Human Beta Cells. Cell Metab. 29, 638–652.e5.

Wiklund, S., Johansson, E., Sjöström, L., Mellerowicz, E.J., Edlund, U., Shock-cor, J.P., Gottfries, J., Moritz, T., and Trygg, J. (2008). Visualization of GC/TOF-MS-based metabolomics data for identification of biochemically interesting compounds using OPLS class models. Anal. Chem. 80, 115–122.

Wu, Y., Williams, E.G., Dubuis, S., Mottis, A., Jovaisaite, V., Houten, S.M., Arg-mann, C.A., Faridi, P., Wolski, W., Kutalik, Z., et al. (2014). Multilayered genetic and omics dissection of mitochondrial activity in a mouse reference population. Cell 158, 1415–1430.

Xu, W., Zhu, H., Gu, M., Luo, Q., Ding, J., Yao, Y., Chen, F., and Wang, Z. (2013). DHTKD1 is essential for mitochondrial biogenesis and function mainte-nance. FEBS Lett. 587, 3587–3592.

Yamanaka, M., Itakura, Y., Inoue, T., Tsuchida, A., Nakagawa, T., Noguchi, H., and Taiji, M. (2006). Protective effect of brain-derived neurotrophic factor on pancreatic islets in obese diabetic mice. Metabolism 55, 1286–1292.

Zeng, L., O'Connor, C., Zhang, J., Kaplan, A.M., and Cohen, D.A. (2010). IL-10 promotes resistance to apoptosis and metastatic potential in lung tumor cell lines. Cytokine 49, 294–302.

Zhou, P., She, Y., Dong, N., Li, P., He, H., Borio, A., Wu, Q., Lu, S., Ding, X., Cao, Y., et al. (2018). Alpha-kinase 1 is a cytosolic innate immune receptor for bacterial ADP-heptose. Nature 561, 122–126.

STAR★METHODS

KEY RESOURCES TABLE

REAGENT or RESOURCE	SOURCE	IDENTIFIER
Antibodies		
Primary antibody Insulin	Ozyme	Cat# C27C9; RRID: AB_2687822
Primary antibody Glucagon	Ozyme	Cat# 2760S; RRID: AB_659831
Primary Anti-Ki 67 antibody	Abcam	Cat# ab15580; RRID: AB_443209
Rabbit Anti-Ki 67 antibody	Abcam	Cat# ab16667; RRID: AB_302459
Secondary Donkey Anti-Goat IgG H&L conjugated to Alexa Fluor® 568	Abcam	Cat# ab175704; RRID: AB_2725786
Primary Mouse/Rat CD31/ PECAM-1 Antibody	R and D System	Cat# AF3628; RRID: AB_2161028
Secondary Goat anti-Rabbit IgG H&L conjugated to Alexa Fluor 488	ThermoFisher	Cat# A-11034; RRID: AB_2576217
Goat anti-rabbit IgG Alexa Fluor 594	ThermoFisher	Cat# A-11037; RRID: AB_2534095
Polyclonal guinea pig anti-insulin antibody	DAKO	Cat# A0564; RRID: AB_10013624
Biological Samples		
Human serum from cardiometabolic patients. Table S2	Lebanese American University, Beirut, Lebanon	N/A
Rat plasma and organs	This paper	N/A
Mouse plasma and organs	This paper	N/A
Chemicals, Peptides, and Recombinant Proteins		
p-cresol	SIGMA	Cat# W233706; Batch MKCD9957
n-Alkane mixture	Restek	Cat# C8-40
Human insulin	Eli-Lilly	Humalog
GLP-1	SIGMA	Cat# G8147; Batch 036M4781V
Critical Commercial Assays		
Insulin ELISA	Eurobio	Stellux 80-INSMR-CH10
Insulin ELISA	Mercodia	https://www.mercodia.com/product/insulin-elisa/
Quantitative RT PCR SYBR green	Eurogentec	https://secure.eurogentec.com/fields-of-studies/mesa-green-qpcr-kits-for-sybr-assay.html
C-peptide ELISA	Crystal Chem	www.crystalchem.com/mouse-c-peptide-elisa-kit.html
Leptin immunoassay	Merck Millipore	www.merckmillipore.com/FR/fr/product/Mouse-Leptin-ELISA,MM_NF-EZML-82K
Ghrelin immunoassay	Merck Millipore	www.merckmillipore.com/FR/fr/product/Rat-Mouse-Ghrelin-active-ELISA,MM_NF-EZRGRA-90K
Liver triglycerides colorimetric assay	Abcam	Cat# ab65336
NAD/NADH quantification	Sigma Aldrich	Cat# MAK037
Experimental Models: Cell Lines		
Pancreatic islets from C57BL/6J mice	This paper	N/A
Experimental Models: Organisms/Strains		
Mouse: C57BL/6J strain	Janvier laboratories	C57BL/6JRj
Rat: Goto-Kakizaki strain	Cordeliers Research Centre	GK/Ox
Oligonucleotides		
Primer for analysis of candidate gene expression. Table S3	This paper	N/A
Software and Algorithms		
GCMS solution software	Shimadzu	Version 2.71

(Continued on next page)

Continued

REAGENT or RESOURCE	SOURCE	IDENTIFIER
β-cell mass quantitative analysis	Golson et al., 2014	N/A
NDP.view2 Viewing software	Hamamatsu	https://www.hamamatsu.com/eu/en/product/type/U12388-01/index.html
Microscopic imaging	Calopix	www.tribvn-hc.com/en/digital-imaging-solutions-applications/calopix/?gclid=CjwKCAiAsIDxBRAsEiwAV76N893AjiRQXDhHH4fh8AwQRV8VPJ6wAlFy5Hg2LflZusV7FrTtea-B6xoCVLAQAvD_BwE
Graphpad 7	GraphPad Software	https://www.graphpad.com
QuPath	QuPath Software	https://qupath.github.io
Other		
Alzet Minipumps model 2006	Charles River Lab France	https://www.alzet.com/products/alzet_pumps/
Mouse diet: Standard chow diet	Research diets	Cat# D12450Ki
Mouse diet: High fat diet	Research diets	Cat# D12492i
Rat diet: Standard chow diet	Safe	Cat# R04-40
Mass spectrometer	Shimadzu	GCMS-QP2010 Ultra
Blood glucose monitoring	Roche Diagnostics	Accu-Check Performa

LEAD CONTACT AND MATERIALS AVAILABILITY

Further information and requests for resources and reagents should be directed to and will be fulfilled by the Lead Contact, Dominique Gauguier (dominique.gauguier@inserm.fr).

This study did not generate new unique reagents.

EXPERIMENTAL MODEL AND SUBJECT DETAILS

Study Subjects

The study population consisted of a total of 137 subjects (89 males and 48 females) recruited between 2006 and 2009 for inclusion in the FGENTCARD patient collection (Saade et al., 2011). Subjects were phenotypically well characterized patients with a mean age of 54.96 (±1.01) years, a mean body weight of 77.84 kg (±1.23) and a mean BMI of 28.04 kg/m^2 (±0.42) (Table S2). They were selected to enter the metabolomic study on the basis of extreme symptoms of cardiometabolic disease (CMD) using measures of plasma HDL cholesterol levels, presence of coronary stenosis and a positive family history of the disease, defined as a sibling, parent, or second-degree relative with a coronary event. Among these, 77 were classified as high CMD risk patients with elevated BMI (> 30kg/m^2) (24%), low plasma HDL cholesterol (< 40mg/dL) (50%) and fasting hyperglycemia (> 125mg/dL) (10%). These were classified as cases (77), while the remaining 60 subjects were classified as control. T2D identification was based on clinical documentation in the patients' medical charts. There were no significant gender differences for any of these phenotypes. Patients provided a written consent for the whole study including genomic analyses. The study protocol was approved by the Institutional Review Board at the Lebanese American University.

Animals

C57BL/6J mice were received from a commercial supplier (Janvier Labs, Courtaboeuf, France). A colony of Goto-Kakizaki (GK/Ox) rats was bred locally. Animals were maintained in specific pathogen free (SPF) condition. They had free access to a standard chow diet (R04-40, Safe, Augy, France) and were kept on 12h light/dark cycle. Minipump experiments were carried out in six-week old male C57BL/6J mice and 32 week-old male GK rats. Islets were prepared from eleven-weeks-old male C57BL/6J mice. All procedures were carried out under national French license condition (Ref 00486.02) and were authorized following review by the institutional ethics committee of the University Pierre and Marie Curie.

METHOD DETAILS

Chemicals

Purified water (TOC grade), methanol (residual PCB grade), chloroform (residual PCB grade), and pyridine dehydrated were purchased from Wako Pure Chemical Industries (Osaka, Japan). Methoxyamine hydrochloride and 2-isopropylmalic acid were obtained from Sigma-Aldrich (Sigma-Aldrich, Tokyo, Japan).

Human serum sample preparation

The internal standard solution (2-isopropylmalic acid, 0.1 mg/mL in purified water) and extraction solvent (methanol: water: chloroform = 2.5:1:1) were mixed at a ratio of 6:250, which was added to 50 μL of each serum sample. The resulting solution was mixed using a shaker at 1,200 rpm for 30 min at 37°C. After centrifugation at 16,000 x g for 5 min at 4°C, 150 μL of supernatant was collected and mixed with 140 μL of purified water. The solution was thoroughly mixed and centrifuged at 16,000 x g for 5 min at 4°C. Finally, 180 μL of supernatant was collected and lyophilized. The lyophilized sample was dissolved in 80 μL of methoxyamine solution (20 mg/mL in pyridine) and agitated at 1,200 rpm for 30 min at 37°C. Forty micro litters of N-methyl-N-trimethylsilyltrifluoroacetamide solution (GL science, Tokyo, Japan) were added for trimethylsilyl derivatization, followed by agitation at 1,200 rpm for 30 min at 37°C. After centrifugation at 16,000 x g for 5 min at room temperature, 50 μL of supernatant was transferred to a glass vial and subjected to GC-MS measurement.

Gas chromatography coupled to mass spectrometry (GC-MS)

GC-MS analysis was performed using a GCMS-QP2010 Ultra (Shimadzu, Kyoto, Japan). The derivatized metabolites were separated on a DB-5 column (30 m x 0.25 mm id, film thickness 1.0 μm) (Agilent Technologies, Palo Alto, CA). Helium was used as the carrier gas at the flow rate of 39 cm/sec. The inlet temperature was set on 280°C. The column temperature was first held at 80°C for 2 min, then raised at the rate of 15°C/min to 330°C, and held for 6 min. One micro litter of the sample was injected into the GC-MS in the split mode (sprit ratio 1:3). The mass condition was as follows: electron ionization mode with the ionization voltage: 70 eV, ion source temperature: 200°C, interface temperature: 250°C, full scan mode in the range of m/z 85-500, scan rate: 0.3 s/scan. Data acquisition and peak processing were performed with a GCMS solution software Version 2.71 (Shimadzu, Kyoto, Japan).

Targeted metabolomic data analysis

Chromatographic peaks were identified by comparing their mass spectral pattern to those in the NIST library or Shimadzu GC/MS Metabolite Database Ver. 1. The identification of metabolites was further confirmed through the coincidence of retention indices in samples with those in the corresponding authentic standards. Retention indices were determined and calibrated daily by the measurement of n-Alkane mixture (C8-40) (Restek, Tokyo, Japan), which was run at the beginning of batch analysis. A total of 101 metabolites were identified. Quantitative ions were selected for area calculation (summarized in Table S1) and the peak area of each metabolite was normalized.

Animal experiments

A group of 12 six-week old C57BL/6J male mice was fed control carbohydrate diet (CHD) (D 12450Ki, Research diets, NJ) and a group of 12 mice was fed high fat (60% fat and sucrose) diet (HFD) (D12492i, Research diets, NJ). One week later mice were anaesthetized with isoflurane and osmotic minipumps Alzet® model 2006 (Charles River Lab France, l'Arbresle, France) filled with the metabolites 4-cresol or 4-methylcatechol (6 CHD-fed and 6 HFD-fed mice) (5.55mM in 0.9% NaCl) (Sigma Aldrich, St Quentin, France) or with saline (6 CHD-fed and 6 HFD-fed mice) were inserted subcutaneously on the dorsal left side (Figure S1). Concentration of these metabolites was adjusted for a flow rate of 0.15μL/h. The selected dose of 4-cresol was determined following a toxicology study of the effects of repeated subcutaneous injections 4-cresol over a period of 14 days (data not shown). The same procedure was applied to insert the minipumps filled with 4-cresol (5.55mM in 0.9% NaCl) or saline subcutaneously in 32 week-old male GK rats.

Blood glucose and body weight were monitored weekly during the 6-week long administration of 4-cresol or saline. After three (mice) or four (rats) weeks of treatment (i.e., four weeks of HFD feeding in mice) an intraperitoneal glucose tolerance test (IPGTT) (2g/kg in mice, 1g/kg in rats) was performed in conscious animals following an overnight fast. For the IPGTT carried out in mice, blood was collected from the tail vein before glucose injection and 15, 30, 60 and 120 minutes afterward. Additional blood samples were collected during the IPGTT in GK rats 15, 90, 180 and 240 minutes after glucose injection. Blood glucose levels were determined using an Accu-Check® Performa (Roche Diagnostics, Meylan, France). Additional blood samples were collected at baseline and 30 minutes after glucose injection in Microvette® CB 300 Lithium Heparin (Sarstedt, Marnay, France). Plasma was separated by centrifugation and stored at −80°C until insulin and C-peptide assays. Evaluation of overall glucose tolerance was obtained from the cumulative glycemia (GCum) and the ΔG, which were determined by the total increment of plasma glucose values during the IPGTT (GCum) and the cumulative glycemia during the test above baseline (ΔG).

To assess insulin sensitivity in mice treated with 4-cresol or 4-methylcatechol, insulin tolerance tests (ITT) were performed in conscious animals after four weeks of metabolite infusion (i.e., five weeks of HFD feeding). Mice were fasted for 5 hours before receiving an intraperitoneal injection of insulin (0.5 U/kg; Humalog) (Lilly, Neuilly-sur-Seine, France). Glycemia was measured before insulin injection and 15, 30, 45, 60, 90 and 120 minutes afterward.

After six weeks of metabolite treatment, animals were killed by decapitation and organs were dissected and weighed. Half of liver, fat and pancreas samples were snap frozen in liquid nitrogen and stored at −80°C for molecular studies, and the second half processed for histopathology.

A replication study was later carried out in CHD and HFD-fed C57BL/6J mice treated with 4-cresol or 4- methylcatechol (four mice per group) using the same experimental procedure as above in addition to records of food intake. Daily food intake was recorded in individually housed mice over a period of two consecutive days after 10 days of treatment with the metabolites and following a 24-h

acclimatization period. Energy intake was calculated by multiplying the amount of food consumed by energy density (5.21 kcal/g for high fat diet and 3.82kcal/g for chow diet).

Histology and immunohistochemistry of animal tissues

Tissues were drop-fixed in 4% paraformaldehyde (Sigma-Aldrich, Saint Quentin Fallavier, France) immediately after collection and put through an automated carousel processor for dehydration, clearing and paraffin embedding (Leica, Nanterre, France). Tissue sections from all animals used in the study were prepared. Sections of liver (6 μm), pancreas (6 μm) and adipose tissue (10 μm) were mounted on slides (DPX polymerizing mountant, Sigma-Aldrich, Saint Quentin Fallavier, France) and stained with Hematoxylin and Eosin (H&E). Epitope-specific antibodies were used for immunohistochemistry detection of insulin on pancreas sections (Dako, Saint Aubin, France).

For Oil red O (ORO), livers were snap frozen in OCT (VWR, Fontenay-sous-Bois, France) and cut into 7μm sections using a cryostat. Sections were rehydrated in PBS (Sigma-Aldrich, St Quentin, France) and incubated with an ORO staining solution (Sigma Aldrich, St Quentin, France). Slides were washed in deionized water and mounted with Vectashield mounting medium (Eurobio, Les Ulis, France).

For immunohistochemistry analysis, pancreas sections were quenched with 3% H_2O_2, washed with TBS + 0.1% (v/v) Tween-20 (or 0.05% v/v Triton X-100 for nuclear epitopes), blocked with TBS + 3% (w/v) BSA and incubated with diluted primary antibodies (Insulin C27C9 and Glucagon 2760S, Ozyme, Saint-Cyr-l'École, France) and then with HRP-conjugated secondary antibody (Fisher Scientific Illkirch, France, Bio-Rad, Marnes-la-Coquette, France). Chromogenic detection was carried out with the DAB chromogen kit (Dako, Saint Aubin, France). Nuclei were counterstained with hematoxylin. Quantitative expression of all immunostainings was performed using positive pixels algorithm (Indica Labs, Corrales, NM). For double immunostaining and immunofluorescence analyses, pancreas sections were stained for insulin as described above and co-stained with i) primary Anti-Ki 67 antibody (ab15580) (Abcam, Paris, France) and secondary Donkey Anti-Goat IgG H&L conjugated to Alexa Fluor® 568 (ab175704) (Abcam, Paris, France) ii) primary Mouse/Rat CD31/PECAM-1 Antibody (AF3628) (R and D Systems, Minneapolis, MN) and secondary Goat anti-Rabbit IgG H&L conjugated to Alexa Fluor 488 (A-11034) (ThermoFisher, Villebon, France). Results are expressed as percentage of positive pixels, within islets where indicated. The quantification method is an automated observer-independent process based on section scanning and application of publicly available algorithms. Each biological replicate represents one slide per animal mounted with at least 3 tissue sections, representing 3 technical replicates, the mean and variance of which is presented as the result per biological replicate. β-cell mass was determined on pancreatic serial sections using a published algorithm (Golson et al., 2014), taking into account the recorded weight of total pancreas in the animals. All images were acquired on an Axiovert 200M microscope (Zeiss, Marly-le-Roi, France).

In vitro insulin secretion in mouse isolated islets

Eleven-weeks-old male C57BL/6J (Janvier-Labs, Saint-Berthevin, France) were killed by cervical dislocation. A solution of collagenase (0.65mg/ml) (Roche, Sigma Aldrich, St Quentin, France) dissolved in a buffer containing Hanks (HBSS) (GIBCO Invitrogen, Saint-Aubin, France), HEPES (0.01M) (GIBCO Invitrogen, Saint-Aubin, France) and DNase I (0.1mg/ml) (Sigma Aldrich, St Quentin, France) was injected through the bile duct. Pancreas was dissected and incubated at 37°C in a collagenase solution. The reaction was stopped by addition of a cold buffer containing HBSS, BSA (0.5%) (Interchim, Montluçon, France) and HEPES (0.024M). Islets were purified on a four layer density gradient of Histopaque 1119 (Sigma-Aldrich, St Quentin, France) and HBSS, and incubated overnight at 37°C in RPMI (GIBCO Invitrogen, Saint-Aubin, France) mixed with HEPES (10mM), sodium pyruvate (1mM) (GIBCO Invitrogen, Saint-Aubin, France), beta-mercaptoethanol (0.05mM), gentamicin (0.1mg/ml) (Sigma Aldrich, St Quentin, France) and FBS 10% (Eurobio, Les Ulis, France). Islets were then split into three groups incubated for 24 hours with either the culture medium (controls) or with cresol (10nM or 100nM) (W233706, Sigma Aldrich, St Quentin, France). *In vitro* insulin secretion tests were performed after 48 hours of 4-cresol treatment. Islets were pre-incubated in KRBH-0.05% BSA with 2.8mM of glucose for 30 min, followed by 60 min incubation in KRBH-0.05% BSA with 2.8 or 16.7mM glucose to measure glucose-induced insulin secretion in absence of 4-cresol or in presence of 4-cresol 10nM or 100nM. Insulin was determined on supernatant by ELISA (Eurobio, Les Ulis, France). A batch of islets was used to determine insulin content.

Analysis of β-cell proliferation *in vitro* in mouse isolated islets

Islets were isolated and purified from 16 week old C57BL/6J mice (Janvier-Labs, Saint-Berthevin, France) as above described. Islets were dispatched by handpicking at a density 50 islets in Petri dishes and maintained overnight at 37°C in a stabilization culture medium containing RPMI1640 supplemented with HEPES (10mM), glutamine (2mM), Penicillin (100U/ml), Streptomycin (100 μg/ml) and 10% SVF. Islets were then incubated for 48 hours in a medium free of 4-cresol or containing either 4-cresol (10nM or 100nM) the effective dose (ED) of GLP1 (10nM) or the median effective dose (ED_{50}) of GLP-1 (10nM (Sigma Aldrich, St Quentin, France). 4-Cresol and GLP-1 were prepared in H2O and diluted in RPMI1640 completed with 10% SVF to achieve the final expected tested concentration. Media were changed every 24h. Experiments were carried out in four batches of 50 islets (controls) and in three batches of 50 islets for the groups treated with 4-cresol or GLP-1. Then 40 islets were collected for each condition, washed in Dulbecco's phosphate-buffered saline (DPBS, Sigma Aldrich, St Quentin, France) and digested by Trypsin-EDTA 0.25%. Cytospin was carried out on 40 islets fixed in paraformaldehyde 3.7% and permeabilized with Triton X-100 - 0.2% in BSA 5%. Islets

were stained with a rabbit anti-Ki67 antibody (Abcam, Paris, France) coupled with goat anti-rabbit IgG Alexa Fluor 594 (ThermoFisher Scientific, Villebon, France) and a polyclonal guinea pig anti-insulin antibody (Agilent DAKO, Courtaboeuf, France) coupled with anti-guinea pig antibody conjugated with FITC. Cell nuclei were stained using Hoechst 33342 (ref. H3570) (ThermoFisher, Villebon, France). The number of cells stained with Ki67 immunostaining was determined after slide scanning and analysis with NDP view imaging software and Calopix Software. Scanning was performed on 3 slides per condition. A minimum of 6,000 cells per treatment in randomly selected fields were counted.

RNA isolation and quantitative RT-PCR

RNA was extracted from pancreas, adipose tissue and isolated islets using the RNeasy RNA Mini Kit (QIAGEN, Courtaboeuf, France). Reverse transcription was performed from a 20 μL reaction mixture with 500 ng RNA using M-MLV reverse transcriptase kit (ThermoFisher, Villebon, France). Quantitative RT-PCR was performed using sequence specific primers and the MESA green kit for SYBR green assays (Eurogentec, Angers, France). We used 18S and/or cyclophilin housekeeping genes to normalize relative quantification of mRNA levels using the Livak and Schmittgen methods (Livak and Schmittgen, 2001). Primers are listed in Table S3.

QUANTIFICATION AND STATISTICAL ANALYSIS

Analytical assays

Blood glucose was measured using an Accu-Check® Performa (Roche Diagnostics, Meylan, France) and plasma insulin was determined using Insulin ELISA kits (Mercodia, Uppsala, Sweden). C-peptide was assayed by ELISA test (Crystal Chem, Elk Grove Village, Il) according to the manufacturer's instructions. Plasma leptin and ghrelin were quantified using an immunoassay (Merck Millipore, Guyancourt, France) according to the manufacturer's instructions. The data were acquired and processed by Luminex technology FlexMap 3D® and the software xPONENT® 4.2 (Merck Millipore, Guyancourt, France). For determination of liver triglyc-erides, liver samples (100mg) were homogenized and incubated in Nonidet P-40 (5%) and supernatants containing triglycerides were collected. Triglycerides concentration was quantified in the supernatant fraction using a colorimetric assay (ab65336, Abcam, Paris, France) by measuring OD at 570nm. The ratio NAD/NADH was determined using a quantification kit (MAK037; Sigma Aldrich, St Quentin, France) on extracts prepared from 20 mg pancreas tissue. Samples were homogenized in the extraction buffer and clarified by centrifugation. Supernatant was deproteinized by filtration through a 10-kDa cutoff spin filter (Millipore SAS, Molsheim, France). The assay was then performed according to the manufacturer's instructions.

Statistical analyses

A linear regression model was applied to the statistical analysis of the metabolomic dataset to assess association of each metabolite with Type 2 diabetes. Normality assumption of the residuals of each metabolic feature was investigated by Shapiro-Wilk test. The R statistical language was then used to perform the linear regression and compute a P value for each metabolic feature with a threshold of significance set to 0.05. Analyses were adjusted for age and gender effects. Statistics were calculated using two-way ANOVA, two-tailed Student t test or Mann Whitney test. Differences were considered statistically significant with a $p < 0.05$.

Multivariate modeling of the metabolic signature related to type 2 diabetes was performed through Orthogonal Partial Least-squares Discriminant Analysis (O-PLS-DA) using the R package ropls version 1.10.0. Briefly, 2-Oxobutyric_acid was removed from the following analysis due to high proportion of zero values (0.5255), then a value of 0.0001 was given to each zero value of other metabolites, and natural logarithm transformed. The resulted matrix of 137 samples with 100 metabolites was applied to O-PLS-DA analysis after the values were mean-centered and scaled. Goodness-of-prediction (Q2) value was calculated by 7-fold cross validation, and the significance of R2 and Q2 was estimated by 10,000 times permutation.

DATA AND CODE AVAILABILITY

This study did not generate any unique datasets or code.